American Mineralogist, Volume 100, pages 2518–2532, 2015

Weathering of the Ethiopian volcanic province: A new weathering index to characterize and compare soils† 🔓

Jennifer S. Le Blond[1,2,*], Javier Cuadros[2], Yordanos B. Molla[1,3], Tadesse Berhanu[3], Mohammed Umer[3,‡], Peter J. Baxter[4] and Gail Davey[1]

[1]Brighton and Sussex Medical School, University of Sussex, Brighton, East Sussex BN1 9PX, U.K.
[2]Department of Earth Sciences, Natural History Museum, London SW7 5BD, U.K.
[3]Department of Earth Sciences, Addis Ababa University, Addis Ababa 1000, Ethiopia
[4]Institute of Public Health, University of Cambridge, Cambridge CB2 2SR, U.K.

Abstract

Soil formation occurs through numerous physical and chemical weathering processes acting to alter the parent rock on the Earth's surface. Samples of surface soils were collected over a range of elevations (2000–3600 m) from profiles directly overlying basaltic to more felsic parent rocks, over a region in NW Ethiopia. The soils were investigated to determine their chemical composition and X-ray diffraction was used to identify and quantify individual mineral phases. The data set was analyzed using non-parametric statistics (Spearman's Rank and Mann-Whitney U tests) to compare the soils forming over the two parent rocks. Principal component analysis (PCA) was used to identify the mineral alteration assemblage and formation during pedogenesis. The extent of alteration was quantified using several chemical weathering indices (Chemical Index of Alteration = CIA; Chemical Index of Weathering = CIW), including an index calculated by multivariate analyses of the soil chemical composition data (weathering "*W*" index). Further to this we devised and tested a new weathering index (W_{min}) using multivariate analysis of the soil mineralogy, to estimate the extent of weathering and physico-chemical proprieties of the parent rock from which the soil formed.

The soils present a fair to advanced stage of alteration, with abundant iron (Fe) oxides (up to 40 wt%) and phyllosilicates (up to 57 wt%), including kaolinite-smectite (K-S) mixed-layer phases. The K-S was composed of either 30–50% kaolinite or 94–98% kaolinite layers. Discrete kaolinite was also present. The bimodal K-S mineralogical composition is likely due to two precursor phases: feldspar for the kaolinite-rich K-S and volcanic glass for the smectite-rich K-S. K-S with intermediate composition (50–94% kaolinite) was rare, due to its instability. Statistical analysis showed significant differences between the chemical compositions of the soils developed on the two different parent volcanic compositions. The soils overlying the more felsic parent rocks were less altered than those overlying the flood basalt. When comparing the weathering indices calculated in this study, we conclude that while the CIA and CIW may be more readily determined, the *W* and W_{min} indices can elucidate information on the composition of the original rock from which they formed. The *W* index is more sensitive to certain variables when compared with the newly derived mineralogical W_{min} index; however the W_{min} index takes into account mineral phases within the sample, which provides a more detailed interpretation of weathering rates than chemistry alone. In addition the W_{min} index correlated with meteorological variables, such as elevation (and consequently temperature and precipitation), known to influence the degree of pedogenesis. The W_{min} index can be used to enhance our understanding of the processes that occur during weathering processes to supplement information gained from traditional chemical weathering indices.

Keywords: Soils, pedogenesis, weathering, basalt, multivariate statistics, principal component analysis (PCA)

Introduction

The formation of soils (pedogenesis) is a process by which weathering alters constituents within the parent deposit through the loss of more mobile (i.e., soluble) elements, concurrent enrichment of less mobile elements, combined with alteration and formation of new secondary minerals and accumulation of organic matter. The rate and extent of pedogenesis is highly dependent on a range of factors, including the lithology of the parent material, climatic conditions, time, presence of organisms within the strata, vegetation, and topography (e.g., Jenny 1941).

Extrusive igneous rocks are thought to be particularly sensitive

* E-mail: j.le-blond@imperial.ac.uk
‡ Mohammed Umer died suddenly during the course of this study.
† 🔓 Open access: Article available to all readers online.

to chemical erosion (Berner and Berner 1996), weathering 5–10 times faster than intrusive crystalline rocks (such as granite; Dessert et al. 2001). Furthermore, the weathering of mafic (basaltic) minerals is more rapid than that of felsic minerals (e.g., Sigfusson et al. 2008). Basaltic rocks are composed of primary minerals, mesostasis, and glass that, over time, develop into soils with comparably more stable mineral phases at surface conditions. Geochemical weathering of basalt begins with the loss of non-hydrolyzing cations (such as calcium, magnesium, and sodium) and the concomitant enrichment of silicon, aluminum, and iron ions in both crystalline and non-crystalline phases (Chorover et al. 2004). In terms of mineralogy, weathering typically removes the primary silicate phases (and glass), and replaces them with poorly crystalline aluminosilicates. Weathering can eventually produce iron oxide and oxyhydroxide phases that evolve toward more crystalline varieties (e.g., Rasmussen et al. 2010; Dahlgren et al. 2004; Righi et al. 1999).

Large igneous provinces are regions of extensive crustal emplacements of extrusive igneous rock, and one such example is the Ethiopia Volcanic plateau (EVP): a vast area (~0.81×10^6 km^2; Dessert et al. 2003) igneous deposit in modern day Ethiopia. The EVP was formed when extensive eruptions deposited ~350 000 km^3 of basalt (flood basalt; marking the appearance of the Ethiopian-Afar plume superswell) over a <2 Ma period (Mohr 1983; Mohr and Zanettin 1988). Several large shield volcanoes subsequently developed on the surface of the flood basalt (Mohr and Zanettin 1988), which in turn produced ~$^1/_5$ of the total volume of basaltic lava distributed in discrete outcrops across the flood basalt. Deposits from these (younger) shield volcanoes are generally more felsic, thinner, and less continuous than the extensive flood basalts that they cover. Mt. Choke is a shield volcano located in the center of the EVP, 215 km NW of Addis Ababa (Fig. 1), in the Gojam region. Mt. Choke (elevation 4052 m) stands ~1200 m above the surrounding flood basalts and the upper 300–400 m of the Mt. Choke sequence contains deposits that are more felsic than the surrounding flood basalts (Fig. 1). $^{40}Ar/^{39}Ar$ dating of a rhyolitic sample near the summit has provided an estimate of the age of the summit deposits of 22.4 (± 0.3) Ma (Kieffer et al. 2004). The Mt. Choke shield volcano is divided into six main deposits, differentiated by their igneous characteristics, from the summit to the base: Choke peak basalt, Choke rhyolite, Kutye basalt, Choke trachyte plug, Arat Mekeraker basalt and Rob Gebaya basalt (Fig. 1). The older, surrounding flood basalts are 25–29 Ma old (Hofmann et al. 1997), and are divided into four main deposits: Lumame, Debre Markos, Yejube, and Arero Gidabo basalts.

The soils near the summit of Mt. Choke are typically lighter and grayish brown in color, whereas soils at lower elevations of Mt. Choke and on the flood basalts are characteristically reddish brown. The soil units covering Mt. Choke have been classified as Haplic Alisols (deep soils with a predominantly clay or silt-clay texture), Eutric Leptosols (shallow soils with loam or clay-loam texture), and Eutric Vertisols (deep soils with clayey texture and angular/sub-angular blocky structure) (BCEOM 1999). The soil cover on Mt. Choke region is heavily influenced by morphological activity (e.g., erosion and land sliding), and calculations from remote sensing estimate that the soil thickness (i.e., depth to bedrock) varies from nonexistent to several meters (Teferi et al. 2010). The endemic natural forest cover in the Mt. Choke region has been predominantly replaced with grasslands and moorland, with patches of woody plant cover and ever-increasing plantations of Eucalyptus (*Eucalyptus globulus*). Isolated family-owned and worked fields are widespread, growing wheat, teff (*Eragrostis tef*), or other agricultural crops. Erosion rates are relatively high, and it is estimated that the farmed highland areas above the central and eastern parts of the basin are a major sediment source into the Blue Nile (Bewket and Teferi 2009). Soil degradation, both erosion and decreasing fertility, is a recognized problem in the Ethiopian Highlands (e.g., Van de Wauw et al. 2008). The majority (80–85%) of the Ethiopian population work within the agricultural sector (Alemayehu 2003), and the quality of the soil is continuously declining due to the intensification of cultivation driven by factors such as population increase and a need to increase food yields in times of drought (Devereux 2000).

The mineralogy and geochemistry of the surface soil can potentially offer an insight into the weathering process and various chemical alterations that have occurred to change the parent rock and regolith over time on the EVP. The parent material is found below the soil as unaltered, pristine rock. Increasing alteration is observed toward the upper soil layer, within the O and A horizons, typically subjected to the most intensive weathering processes. Geochemical-based weathering indices are commonly used to measure and compare the relative extent and intensity of soil pedogenesis based on the chemistry of the surface soils. In theory, the ionic potential of elements in the rock or soil determines whether the element is soluble and thus the extent to which the element will be mobile during weathering. Conventional chemical weathering indices (e.g., Chemical Index of Alteration = CIA; Nesbitt and Young 1982, Chemical Index of Weathering = CIW; Harnois 1988) are based on the chemical composition of the sample and aim to quantify the selective removal of mobile and soluble elements.

The use of standard weathering indices (CIA, CIW, etc.), however, may be restrictive and often not able to account for the changes occurring during real weathering scenarios (e.g., Duzgoren-Aydin and Aydin 2003; Price and Velbel 2003; Duzgoren-Aydin et al. 2002), as they do not consider the subtle variations (for example mineral or chemical heterogeneity) within the parent rock or the variable (often unpredictable) behavior of some components within the soil (for example iron). In situations where the parent rock is heterogeneous over a relatively small volume, conventional chemical weathering indices may not be sensitive enough to recognize subtle compositional differences within the soil that are associated with the parent rock. To derive a value to represent the degree of weathering within soils more accurately, Ohta and Arai (2007) used principal component analysis (PCA: a multivariate analysis tool, used primarily for exploratory data analysis), based on eight main oxides of both mobile and immobile elements (Al_2O_3, CaO, Fe_2O_3, K_2O, MgO, Na_2O, SiO_2, TiO_2). They derived a weathering index "*W*" for soils and sediments forming over igneous rocks. The *W* index has been shown to be a good indicator of the bulk geochemical alterations that occur during weathering, irrespective of igneous parent rock (e.g., Szilas and Garde 2013; Ohta and Arai 2007), which has the advantage of allowing comparative measurement of the degree of weathering between unrelated samples. In addition to igneous rocks, the *W* index has been applied to 3.75 Ga metamorphic mafic-ultramafic rocks with good results (Nuvvuagittuq Greenstone Belt, Hudson

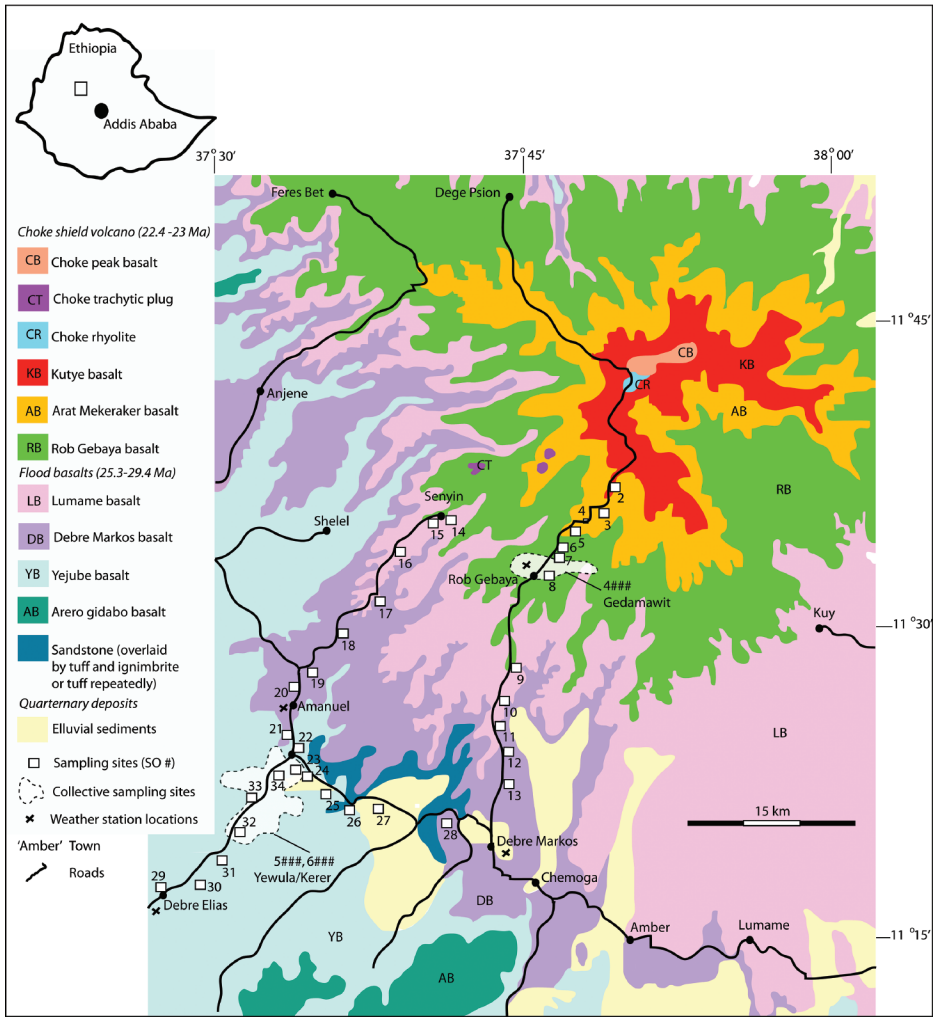

FIGURE 1. Map of the sampling area on the Ethiopian plateau, indicating the locations of the flood basalt deposits, Mt. Choke volcanic shield deposits and sampling sites. Geological Survey of Ethiopia, Debre Markos sheet map, NC37-6, age data from Hofman et al. (1997), Coulié et al. (2003), and Kieffer et al. (2004).

Bay, Canada; O'Neil et al. 2011). Calculation of the *W* index, however, has not proven to be entirely suitable for sedimentary parent rocks (e.g., Zhang et al. 2014), and further testing of this index is justified.

The main objective of this study was to investigate the extent of the weathering and alteration that has contributed to pedogenesis in one region of the EVP. Samples of surface soils were collected and the inorganic components were analyzed, using weathering indices, to reveal the processes of soil formation and extent of alteration over a range of elevations and differing parent rocks. As a second goal, the surface soils over the differing parent rocks were compared to identify whether the parent rock influenced the chemistry and mineralogy of the surface soils. To address these objectives, a new weathering index was developed, derived from the statistical theory given in Ohta and Arai (2007) although based on mineralogy rather than chemistry, which can be used to gain information on both the relative extent of weathering and the igneous nature of the parent rock. When investigating the formation of soil from igneous deposits the use of a weathering index based on soil mineralogy as well as the more conventional weathering indices derived from soil chemistry, can provide additional information that enhances our understanding of pedogenesis.

EXPERIMENTAL METHODS

Meteorological data

Meteorological data was sourced from http://www.WorldClim.org (accessed: February 2014; Hijmans et al. 2005), which generates data layers of interpolated average monthly climate information from weather stations on a 30 s resolution grid (from data gathered between 1950 and 2000). The mean annual precipitation (MAP) and mean annual temperature (MAT) were determined for every sample location using ArcGIS (ArcMap 10.1) (Table 1).

Sample collection

Surface soil samples (n = 135) were collected over the Mt. Choke region of the EVP, selected to best represent the elevation changes and major geologic formations of the region. Soils were collected from areas that are underlain by two main formations: the Mt. Choke shield deposits (Kutye, Arat Mekeraker, and Rob Gebaya) and

the surrounding flood basalt deposits (Lumame, Debre Markos, and Yejube; Fig. 1). Soils collected from the Mt. Choke shield volcano were sampled at elevations 2874–3597 m, and those collected on the flood basalts at 2147–2943 m. At each site, approximately 1 kg of the surface soil (to a depth of ~5 cm) was collected using a plastic trowel and placed into sterile, airtight sample bags, then double bagged and labeled. The GPS waypoint and elevation was recorded for each sample site.

The soil was homogenized and sub-samples were separated at Addis Ababa University. From this point, samples were shipped to, processed, and analyzed at the Natural History Museum (NHM) in London (unless otherwise stated). Permission to export samples was obtained from Addis Ababa University and the Ethiopian Federal Ministry of Mines and Energy, under a DEFRA soil license granted to the NHM. Once in the U.K., further sub-samples of the soil were separated. Aliquots of the soil were dried at 60 °C for at least 48 h, lightly hand ground with a mortar and pestle, and sieved to <2 mm. Sub-samples for chemical analysis were ground in a Reich agate ball mill and sub-samples for X-ray diffraction (XRD) were further hand ground and passed through a 63 µm sieve.

In addition to the soil samples, whole-rock geochemical data from unaltered parent rock material from across the EVP, collected by Kieffer et al. (2004), were incorporated into the study to allow comparison of the weathered surface soils with parent rock samples. In this study we used data labeled "fresh" to "moderately weathered" (by description in Kieffer et al. 2004) that best represented the Mt. Choke shield and upper flood basalt deposits (the latter taken from the Lima Lion section) (for details see Appendix Table 1[1]). Samples from Kieffer et al. (2004) were chosen to represent unaltered, pristine parent rock samples and will be referred to as "unweathered parent rock" hereafter. Whole rock geochemical data were also sourced from igneous "Certified Reference Materials" (CRMs) to compare the data that we collected with type-examples of igneous rocks. The data from Kieffer et al. (2004) and the CRMs used in the study are presented in Appendix Table 1[1], and plotted onto a TAS diagram in Appendix Figure 1[1] to ascertain their igneous origin.

Chemical analysis

The major elemental composition (oxides) of soil samples was determined (n = 135) using a lithium metaborate flux fusion and dissolution, followed by analysis using inductively coupled plasma–atomic emission spectroscopy (ICP-AES) (detailed in Le Blond et al. 2008). At least 1 blank was run for every 5 samples to check for background/cross-contamination. The accuracy and precision of the ICP-AES analysis was measured by regularly analyzing synthetic solutions containing known levels of the elements of interest from the following CRMs: BEN basalt, BHVO-1 basalt, BCR-2 basalt, AGV-1 andesite, GSP-1 granidiorite, JG-1 granidiorite, biotite, NIM-G granite, NIM-P pyroxenite, and STM-1 syenite. Limits of detection (LOD) and limits of quantification (LOQ; in parentheses) are as follows (in wt%): Al_2O_3 0.3(1.1); CaO 0.4(1.3); Fe_2O_3 0.3(1.0); K_2O 0.02(0.06); MgO 1.1(0.4); MnO 0.004(0.01); Na_2O 0.2(0.7); P_2O_5 0.01(0.04); SiO_2 1.5(4.7); TiO_2 0.3(1.0).

Mineralogy

X-ray diffraction (XRD) analysis enables identification and quantification of crystalline components in a bulk, powdered sample. Initially, for phase identification, the soil samples (n = 100) were close-packed into aluminum side-loading sample holders (to favor random orientation of the particles) and analyzed in an Enraf-Nonius X-ray diffractometer with an INEL curved position-sensitive detector (PSD). This apparatus collects data from 2–120 °2θ continuously throughout the measurement. The apparatus used Cu$K\alpha$ radiation (λ = 1.5418 Å), at a voltage of 45 kV and current of 40 mA, with a primary slit of 0.1 mm by 5 mm. Samples were analyzed for 60 min.

The phases identified in the soils were quartz, feldspars, poorly crystalline Fe oxides, smectite, mica, chlorite, amorphous silica, and kaolin-group minerals. The quantification method is detailed in Cressey and Schofield (1996) and Cressey (1999), but briefly, standard mineral samples (from the collections at the NHM) representing those in the soils, were analyzed under identical preparation and instrument conditions. These standards were: a mixture of anorthite, albite, and orthoclase in equal proportions to represent the feldspars; goethite for the poorly crystalline Fe oxides; quartz; and volcanic glass for the amorphous silica phase. The proportion of each of the above mineral phases was determined by matching the contributions of the mono-mineralic standards to the experimental patterns and then correcting the values using the individual mineral X-ray absorption coefficients. The sum of the phyllosilicates (smectite, kaolinite, mica, and chlorite) was determined by difference. The proportion of the individual phyllosilicates was investigated in oriented mounts (see below). Repeated preparation and analysis of a sub-sample set (n = 15) produced quantification values within 5% for all mineral phases.

To investigate the octahedral configuration of the clays (trioctahedral vs. dioctahedral), the 060 peaks were studied. The samples used in the bulk identification XRD analysis were analyzed in the 59–64 °2θ angle range on a PANalytical X'Pert-PRO scanning XRD (240 mm radius) with a step size of 0.0167 °2θ, for a total counting time of 60 min. Cu$K\alpha$ radiation was used, with a voltage of 45 kV and current of 40 mA. The incident beam passed through a 0.02 rad Soller slit, a 1° divergence slit, a 10 mm fixed mask and a 2° fixed anti-scatter slit. The instrument was fitted with a Ge monochromator and the diffracted beam was detected by an X'Celerator RTMS detector.

For the detailed investigation of the phyllosilicates, an aliquot of each of the samples was prepared as an oriented mount on a glass slide. This technique encourages preferred orientation of the clay particles parallel to the glass slide surface and enhances the intensity of the basal reflections (00l). A suspension of soil was prepared (4 mL deionized water was added to 80 ± 0.003 mg sample), sonicated for 1 min and 0.5 mL dropped onto a clean glass slide and left to dry. The PANalytical X'Pert-PRO diffractometer was used, set up as in the analysis of the 060 peaks, but the scan range was 2–60 °2θ, the step size 0.0334 °2θ and a total counting time of 60 min. Once the slides had been analyzed in air-dry conditions, they were glycolated (in a desiccator with ethylene glycol; in an oven at 60 °C for 24 h) to investigate the presence of swelling clays (smectite or vermiculite). The glycolated slides were analyzed using identical conditions as adopted for the air dried oriented mounts.

The XRD patterns from the glycolated samples were used for modeling and quantifying the phyllosilicate phases within the samples, using CLAYSim (version 1.1.6) from MDI. This program calculates the profiles of the 00l peaks of mixed-layer clays with two components, using chemical and experimental input variables. Up to 10 phases can be added to simulate mineral mixtures within the sample. The calculated patterns were matched to the experimental patterns using the whole pattern profile: peak position and shape, as well as background. The glycolated patterns were chosen for this investigation because their peak positions are more reliable than those from air dried patterns due to changes in relative humidity.

Scanning electron microscopy (SEM)

To further investigate the mechanisms of mineral formation within the soils, two samples (SO 5137 and DM-CM SO 7A) were selected that had high quantities of kaolinite and amorphous silica (alteration products). A LEO VP 1455 scanning electron microscope (SEM) with energy-dispersive X-ray (EDX) detector (Oxford Instruments X-Max detector) was used. The samples were set in a resin block, polished, and carbon coated (~12 nm thickness). Samples were analyzed in high vacuum (15 kV, working distance of 12 mm) with backscattered electrons. EDX analyses were acquired for 1 min and the spectra generated were used to identify the mineral phases.

Statistical data processing

The bulk mineralogy and major oxide composition of the soil samples were compared using the non-parametric statistical analysis test Spearman's Rank correlation. A preliminary assessment of the data was carried out using multivariate regression analysis, to determine whether the individual mineral phases within the soils could be represented as functions of the bulk chemical oxides (e.g., mineral = a+b[oxide1]+c[oxide2]+d[oxide3].... etc.). Each individual mineral phase was assessed as a dependent variable using the chemical composition as predictor variables; collinear variables were excluded from the statistical analysis to avoid the problems of multi-collinearity in the regression analysis.

Two indices of chemical weathering, CIA ($Al_2O_3 \times 100/[Al_2O_3 + CaO^* + Na_2O + K_2O]$; Nesbitt and Young 1982) and CIW ($Al_2O_3 \times 100/[Al_2O_3 + CaO^* + Na_2O]$; Harnois 1988); CaO* denotes the CaO exclusively from silicate minerals and can be applied in samples where the molar ratio of CaO/Na_2O does not exceed 1; McLennan 1993), were calculated from the chemical composition of the soils. In addition, the W index from Ohta and Arai (2007) was calculated from the chemical compositional data of our soil samples and from the data provided by Kieffer et al. (2004). As a further step, we adapted the statistical framework from Ohta and Arai (2007) to calculate a W index value from the soil mineralogy, which we refer to as the "W_{min}" index. The data were first centered log ratio (clr)-transformed (a mathematical function applied to each data point to ensure that the data meet the assumptions of the statistical inference procedure to be used; (Aitchison 1986) using the "Hotelling" package R statistical computing software. Zero values were altered

[1] Deposit item AM-15-115168, Appendix Figures and Tables. Deposit items are stored on the MSA web site and available via the American Mineralogist Table of Contents. Find the article in the table of contents at GSW (ammin.geoscienceworld.org) or MSA (www.minsocam.org), and then click on the deposit link.

TABLE 1. Location, elevation, site information for the soil samples, and type of deposit (CS = Choke shield basalts, FB = flood basalts), plus geochemical and mineralogical data (bdl = below detection limit)

	GPS data (UTM)		Meteorology					Chemical composition (wt%)											Mineralogy (wt%)						
Sample	Easting	Northing	MAP (mm/year)	MAT (°C)	Elev. (m)	Village/Health district	Deposit type	Al_2O_3	CaO	Fe_2O_3	K_2O	MgO	MnO	Na_2O	P_2O_5	SiO_2	TiO_2	FeOOH	Quartz	Amor. silica	Feldspars	Kaolinite	Smectite	Mica	Chlorite
SO 2A	371334	1173986	1657	9.6	3592	Abegira	CS	15.17	2.65	11.05	2.90	1.73	0.26	1.45	1.24	39.87	1.66	17.9	11.2	14.3	28.2	6.7	0.4	14.2	7.1
SO 2D	371352	1174025	1657	9.6	3590	Abegira	CS	16.00	1.01	11.51	2.09	1.13	0.44	1.69	0.90	40.99	1.55	19.3	11.5	14.7	29.0	4.1	0.2	15.4	5.9
SO 3A	370367	1171743	1628	10.2	3488	Kikil	CS	16.38	0.56	13.74	1.47	1.44	0.30	0.45	0.60	43.65	2.90	19.6	38.0	14.3	0.0	2.7	0.1	18.3	7.1
SO 3C	370371	1171754	1628	10.2	3488	Kikil	CS	16.70	0.61	13.65	1.47	1.44	0.31	0.44	0.59	42.38	2.93	20.8	31.3	10.7	28.2	2.9	0.2	3.6	2.3
SO 4A	368737	1171056	1622	10.8	3403	Lay Kokeba	CS	18.75	0.48	18.57	0.92	1.21	0.34	0.31	0.59	37.03	3.51	28.6	9.6	17.5	0.0	27.4	1.4	11.1	4.4
SO 5A	367770	1170193	1600	11.6	3291	Amelameda	CS	17.46	0.33	17.52	1.17	1.14	0.37	0.29	0.56	40.20	3.51	25.5	17.4	11.9	0.0	25.7	1.4	13.5	4.5
SO 5B	367774	1170164	1600	11.6	3291	Amelameda	CS	17.48	0.52	16.48	1.33	1.18	0.36	0.33	0.63	40.02	3.23	25.1	37.4	15.9	0.0	12.1	1.3	5.4	2.8
SO 6A	366659	1168883	1586	12.1	3193	Kendamu	CS	18.16	0.29	20.37	1.09	1.13	0.45	0.24	0.53	39.12	4.09	27.6	12.2	12.4	0.0	24.2	2.5	12.4	8.6
SO 7A	366468	1167849	1559	29.3	3096	Ayeselech	CS	18.69	0.63	15.22	1.11	1.74	0.29	0.32	0.48	40.90	2.65	22.8	21.3	11.3	0.0	25.5	3.9	9.8	5.4
SO 8A	364956	1165802	1543	13.1	2971	Rob Gebeya Town	CS	23.73	0.33	21.53	0.43	0.94	0.43	0.12	0.57	32.93	3.53	39.9	0.0	21.1	0.0	35.1	3.9	0.0	0.0
SO 9A	362592	1158477	1435	14.9	2691	Tekesmany	FB	21.76	0.48	15.42	1.28	0.81	0.28	0.10	0.41	45.52	2.52	23.2	13.0	11.5	30.2	13.4	2.1	6.7	0.0
SO 10A	361460	1155655	1386	15.2	2614	Weyzazer	FB	22.30	0.38	16.95	1.19	0.82	0.35	0.08	0.38	42.16	2.36	25.5	17.4	11.9	0.0	28.8	0.5	15.8	0.0
SO 10B	361471	1155666	1386	15.2	2615	Weyzazer	FB	21.44	0.40	14.39	1.57	1.05	0.34	0.13	0.34	45.30	2.10	21.3	21.8	11.0	0.0	25.5	1.2	16.6	2.8
SO 11A	361651	1151032	1356	15.5	2529	Chirako Amba	FB	19.34	0.34	12.99	1.63	1.04	0.23	0.15	0.47	50.19	2.26	18.8	30.2	10.3	0.0	26.4	0.5	10.6	3.3
SO 12A	362003	1148370	1343	15.7	2509	Yeted	FB	18.52	0.40	13.06	1.72	1.09	0.30	0.19	0.45	50.98	2.23	19.6	28.5	10.5	0.0	24.0	0.5	14.1	2.9
SO 13A	360873	1153142	1371	15.5	2524	Lay Acheber	FB	20.74	0.80	18.59	1.22	0.81	0.34	0.09	0.49	36.35	3.48	27.0	6.5	12.4	0.0	39.9	0.7	13.5	0.0
SO 14A	356627	1171220	1512	14.3	2736	Senyin Town	FB	23.88	0.38	22.96	0.34	0.99	0.55	0.08	0.49	32.29	3.96	33.5	0.0	13.9	0.0	50.1	2.5	0.0	0.0
SO 15A	355436	1170941	1501	15.0	2721	Kokit	FB	20.13	0.21	15.25	1.34	1.11	0.39	0.15	0.46	43.25	2.35	21.6	15.1	11.1	0.0	29.8	0.5	11.0	11.0
SO 15C	355472	1170954	1501	15.0	2717	Kokit	FB	21.65	0.29	16.80	1.34	0.93	0.40	0.11	0.56	42.92	2.59	24.0	24.8	15.8	20.9	11.7	0.2	2.6	0.0
SO 16A	352431	1168268	1466	15.3	2617	Adis Ambia	FB	21.00	0.35	19.28	0.56	0.96	0.29	0.08	0.32	32.49	3.11	32.0	5.8	18.6	0.0	34.6	0.7	6.5	1.7
SO 17A	350450	1164299	1460	14.7	2518	Akile Amiba	FB	19.61	0.33	13.72	1.54	1.17	0.30	0.17	0.38	47.42	2.02	20.5	22.5	10.8	0.0	29.5	0.4	11.1	5.1
SO 18A	347104	1161517	1439	16.2	2471	Atanbesa Mikael	FB	19.92	0.26	12.32	1.52	1.16	0.26	0.14	0.25	47.93	1.82	19.4	32.6	10.4	0.0	32.1	0.6	1.1	3.8
SO 18B	347073	1161514	1439	16.2	2473	Atanbesa Mikael	FB	19.67	0.29	12.32	1.47	1.17	0.26	0.17	0.26	48.58	1.88	19.8	22.2	10.6	23.3	13.5	0.3	7.5	2.9
SO 19A	344502	1158150	1436	15.7	2457	Yelechi	FB	20.75	0.29	12.95	1.64	1.14	0.31	0.10	0.26	48.99	1.87	19.8	24.3	10.6	0.0	30.3	0.5	12.7	1.8
SO 20A	343484	1156547	1428	16.0	2380	Dolima	FB	23.59	0.45	14.57	1.22	0.82	0.21	0.09	0.22	43.50	2.03	23.9	11.4	16.1	0.0	33.4	0.6	14.6	0.0
SO 21A	342650	1152639	1413	16.2	2329	Debuti	FB	21.35	0.87	13.91	1.26	1.01	0.24	0.22	0.23	43.87	2.08	21.3	22.9	10.9	0.0	34.5	0.6	9.9	0.0
SO 22A	343090	1151374	1408	16.0	2296	Sasi	FB	21.06	1.11	14.73	1.18	1.04	0.38	0.30	0.23	42.88	2.47	24.2	11.0	11.7	0.0	36.0	0.6	16.5	0.0
SO 22B	343083	1151319	1408	16.0	2292	Sasi	FB	21.75	0.35	14.83	1.29	0.76	0.29	0.11	0.27	43.96	2.41	22.2	18.7	11.2	0.0	33.0	0.6	14.4	0.0
SO 23A	343196	1149702	1341	17.3	2205	Yewula	FB	19.19	0.62	14.08	1.27	0.78	0.20	0.18	0.28	45.32	2.38	21.3	22.9	10.9	0.0	30.9	0.6	13.5	0.0
SO 24A	344111	1149130	1338	17.3	2177	Yeborena	FB	21.21	0.65	18.14	1.00	1.15	0.36	0.20	0.26	40.91	3.01	25.6	16.2	11.9	0.0	30.9	5.6	9.7	0.0
SO 25A	345821	1147435	1333	17.2	2220	Weyinima	FB	18.82	0.75	19.21	0.73	0.88	0.41	0.22	0.22	40.28	3.58	26.5	15.3	12.2	0.0	22.3	16.9	6.9	0.0
SO 26A	348098	1146022	1338	16.7	2288	Aroge Amba	FB	18.03	1.13	9.68	1.29	1.09	0.19	0.84	0.12	52.26	1.51	16.1	2.1	10.1	13.3	13.1	30.6	14.6	0.0
SO 27A	350676	1146054	1309	16.6	2221	Mutek	FB	16.54	0.94	17.48	0.63	0.88	0.27	0.25	0.20	45.10	3.36	23.6	21.6	11.5	0.0	27.8	13.5	2.2	0.0
SO 28A	356549	1144842	1314	16.6	2345	Debirina Kechinw	FB	20.94	0.76	13.45	1.36	0.85	0.27	0.21	0.27	43.40	2.06	23.2	14.4	11.5	0.0	29.6	0.5	20.9	0.0
SO 29A	331299	1138987	1390	16.9	2199	Eliyas Town	FB	19.28	0.20	12.83	1.44	0.69	0.35	0.17	0.27	48.96	2.30	19.8	24.3	10.6	0.0	33.4	0.6	11.3	0.0
SO 30A	334459	1140328	1381	16.9	2218	Anikarma	FB	19.49	0.52	12.85	1.54	0.77	0.37	0.17	0.28	48.46	2.26	19.9	22.2	10.6	0.0	23.3	0.4	23.7	0.0
SO 31A	336657	1141784	1373	17.0	2214	Wunwuin	FB	19.81	0.30	12.77	1.36	0.69	0.36	0.15	0.22	45.81	2.21	19.8	24.3	10.6	0.0	29.8	0.5	14.9	0.0
SO 32A	337997	1144361	1362	17.2	2200	Zibaguder	FB	19.88	0.29	13.29	1.38	0.71	0.35	0.15	0.25	46.76	2.30	20.4	24.7	10.7	0.0	26.0	0.5	17.6	0.0
SO 33A	339519	1146753	1353	17.3	2166	Kerer	FB	19.05	0.37	12.91	1.36	0.76	0.28	0.18	0.28	47.71	2.37	19.9	22.2	10.6	0.0	28.3	0.5	18.4	0.0
SO 34A	341559	1149073	1364	17.0	2209	Yewula	FB	21.62	0.26	14.26	1.31	0.72	0.25	0.13	0.25	44.82	2.37	21.4	19.6	11.0	0.0	30.7	0.5	16.8	0.0
SO 6150	340655	1145875	1344	17.3	2166	Kerer	FB	20.02	0.25	13.40	1.55	0.77	0.34	0.18	0.35	47.57	2.62	21.6	10.1	16.0	0.0	10.6	1.9	39.7	0.0
SO 6148	340410	1146409	1350	17.3	2183	Kerer	FB	19.76	0.74	12.85	1.52	0.79	0.36	0.20	0.50	46.28	2.66	19.2	28.7	16.8	0.0	7.3	1.2	26.8	0.0
SO 6135	340406	1146424	1350	17.3	2177	Kerer	FB	20.20	0.51	13.43	1.53	0.77	0.38	0.18	0.40	46.86	2.57	19.0	18.2	14.5	0.0	11.9	0.6	35.3	0.5
SO 6129	340406	1146424	1350	17.3	2177	Kerer	FB	18.83	0.82	12.84	1.35	0.71	0.35	0.15	0.77	41.82	2.48	19.8	17.8	9.9	0.0	13.0	2.2	36.8	0.5
SO 6121	346730	1146670	1326	16.9	2156	Kerer	FB	21.84	0.33	13.83	1.59	0.78	0.32	0.16	0.34	46.98	2.55	21.6	10.1	15.4	0.0	8.6	1.5	42.8	0.0
SO 6117	340761	1146851	1287	17.3	2182	Kerer	FB	19.57	0.62	13.27	1.40	0.71	0.36	0.16	0.63	44.96	2.55	21.3	10.4	19.8	0.0	9.7	1.9	34.9	1.9
SO 6038	337312	1145349	1369	17.2	2172	Kerer	FB	19.96	0.38	12.61	1.57	0.79	0.32	0.16	0.40	47.37	2.41	19.4	9.3	14.8	0.0	15.1	3.0	36.2	2.3
SO 6037	337286	1145323	1369	17.2	2147	Kerer	FB	19.96	0.52	12.63	1.82	0.85	0.32	0.16	0.46	48.66	2.44	17.9	28.5	14.0	0.0	11.7	0.6	27.3	0.0
SO 6027	333274	1144297	1375	17.1	2202	Kerer	FB	22.16	0.27	13.38	1.50	0.74	0.31	0.14	0.28	46.60	2.43	20.2	23.6	17.3	0.0	15.8	1.7	21.5	0.0

(Table continues on next page)

TABLE 1.—*CONTINUED*

Sample	GPS data (UTM)		Meteorology					Chemical composition (wt%)										Mineralogy (wt%)						
	Easting	Northing	MAP (mm/year)	MAT (°C)	Elev. (m)	Village/Health district	Deposit type	Al_2O_3	CaO	Fe_2O_3	K_2O	MgO	MnO	Na_2O	P_2O_5	SiO_2	TiO_2	FeOOH	Quartz	Amor. silica	Feldspars	Kaolinite	Smectite	Mica	Chlorite
SO 6015	339485	1146166	1353	17.2	2254	Kerer	FB	18.47	0.70	12.03	1.51	0.77	0.35	0.17	0.54	44.55	2.24	19.2	13.8	14.6	0.0	9.3	0.3	43.8	0.0
SO 6013	339923	1146168	1353	17.2	2177	Kerer	FB	20.15	0.55	13.03	1.45	0.73	0.32	0.14	0.51	44.13	2.52	20.8	9.5	15.2	0.0	9.4	0.4	44.6	0.0
SO 6005	339073	1146510	1353	17.3	2187	Kerer	FB	22.25	0.50	13.45	1.49	0.78	0.31	0.13	0.47	45.60	2.35	20.1	9.4	15.0	0.0	13.6	2.0	40.0	0.0
SO 6004	339055	1146237	1353	17.2	2182	Kerer	FB	18.90	0.60	12.68	1.53	0.74	0.36	0.17	0.47	44.66	2.42	19.0	19.3	14.5	0.0	12.6	0.7	34.1	0.0
SO 6002	339282	1146116	1353	17.2	2184	Kerer	FB	20.19	0.16	13.63	1.45	0.74	0.37	0.21	0.35	50.28	2.65	18.0	26.4	14.0	0.0	18.0	2.4	21.2	0.0
SO 6001	339266	1145960	1353	17.2	2181	Kerer	FB	22.57	0.66	14.46	1.59	0.80	0.34	0.14	0.51	49.66	2.38	20.6	8.8	19.6	0.0	10.7	0.5	38.8	1.0
SO 5173	340889	1151155	1377	16.9	2243	Yewula	FB	18.94	1.31	14.75	1.35	0.91	0.33	0.17	0.70	38.80	2.92	26.0	5.5	16.8	0.0	24.7	3.2	23.8	0.0
SO 5171	340887	1151157	1377	16.9	2238	Yewula	FB	20.54	0.56	15.44	1.24	0.80	0.26	0.13	0.38	39.11	2.57	22.9	15.1	18.4	0.0	10.0	0.4	31.8	1.3
SO 5157	342895	1147117	1339	17.4	2154	Yewula	FB	18.92	0.71	13.05	1.59	0.80	0.33	0.18	0.49	45.83	2.50	17.4	29.1	9.3	0.0	6.3	0.3	36.7	0.9
SO 5148	342761	1147220	1339	17.4	2172	Yewula	FB	22.45	0.27	14.21	1.39	0.75	0.32	0.13	0.35	44.57	2.46	21.5	10.9	15.4	0.0	23.1	3.0	26.1	0.0
SO 5137	336695	1149330	1376	17.3	2164	Yewula	FB	25.12	0.32	15.17	0.95	0.57	0.19	0.07	0.18	43.16	2.76	24.5	13.7	25.7	10.7	11.2	1.4	12.7	0.0
SO 5135	337089	1149531	1376	17.3	2150	Yewula	FB	20.73	0.59	14.03	1.30	0.73	0.28	0.14	0.48	41.63	2.76	23.7	15.3	18.7	0.0	23.3	2.5	16.5	0.0
SO 5129	337364	1149347	1376	17.3	2147	Yewula	FB	19.76	0.63	12.78	1.44	0.78	0.32	0.17	0.45	43.31	2.50	19.5	7.2	14.8	0.0	25.5	2.6	30.4	0.0
SO 5128	337359	1149347	1376	17.3	2165	Yewula	FB	20.17	0.56	18.04	1.05	0.64	0.32	0.11	0.75	35.63	2.89	28.8	5.5	17.7	0.0	15.5	2.8	29.8	0.0
SO 5126	337288	1149618	1376	17.3	2943	Yewula	FB	22.19	0.45	14.52	1.16	0.70	0.22	0.11	0.54	40.08	2.71	23.5	3.0	16.1	0.0	16.4	2.5	38.4	0.0
SO 5107	339206	1149959	1368	17.4	2150	Yewula	FB	20.52	0.39	13.05	1.56	0.77	0.30	0.16	0.38	45.46	2.32	21.5	10.9	15.4	0.0	13.6	2.0	36.5	0.0
SO 5104	339209	1149936	1368	17.4	2649	Yewula	FB	19.19	0.35	12.26	1.29	0.70	0.23	0.14	0.29	39.68	2.20	17.3	21.1	10.1	0.0	15.6	0.9	35.0	0.0
SO 5066	340734	1148069	1351	17.3	2183	Yewula	FB	20.33	0.43	13.25	1.64	0.76	0.31	0.18	0.34	45.48	2.39	20.8	19.5	19.4	0.0	8.4	0.4	31.4	0.0
SO 5077	340587	1148210	1351	17.2	2172	Yewula	FB	19.33	0.60	12.70	1.54	0.78	0.32	0.18	0.46	44.86	2.26	23.1	11.2	15.8	0.0	17.3	3.1	29.4	0.0
SO 5024	342597	1149685	1353	17.1	2225	Yewula	FB	21.16	0.70	13.70	1.74	0.86	0.26	0.13	0.51	43.01	2.36	23.3	7.8	16.0	0.0	9.2	0.3	43.5	0.0
SO 5004	341838	1149302	1365	17.0	2221	Yewula	FB	18.41	0.67	11.47	1.64	0.92	0.27	0.18	0.40	45.93	2.19	22.1	13.4	11.9	0.0	9.1	1.4	41.0	1.1
SO 4196	362680	1165819	1513	13.7	2874	Gedamawit	CS	17.37	0.78	13.39	1.73	1.30	0.36	0.25	0.70	44.02	2.36	19.2	12.2	14.7	18.3	2.5	0.0	30.3	2.8
SO 4195	363119	1165980	1513	13.7	2874	Gedamawit	CS	20.40	0.61	19.52	0.88	0.91	0.45	0.13	0.51	35.16	3.47	27.6	11.5	12.5	0.0	15.0	1.0	31.0	1.5
SO 4140	363451	1165445	1515	13.6	2874	Gedamawit	CS	21.20	0.55	18.96	0.87	0.88	0.36	0.13	0.47	36.42	3.29	28.0	3.3	17.4	0.0	10.7	0.6	38.0	2.1
SO 4139b	363325	1165586	1528	13.4	2884	Gedamawit	CS	19.52	0.98	15.25	1.28	1.16	0.37	0.19	0.86	38.05	2.64	31.2	1.4	18.4	0.0	6.1	0.7	39.6	2.4
SO 4139a	363325	1165586	1528	13.4	2884	Gedamawit	CS	21.53	0.82	17.89	0.92	1.02	0.36	0.13	0.68	34.90	3.05	19.7	18.4	14.7	0.0	28.9	3.2	14.2	0.9
SO 4138b	363538	1165783	1528	13.4	2899	Gedamawit	CS	19.28	0.67	15.63	1.03	1.10	0.48	0.25	1.50	38.62	2.37	23.4	6.3	16.0	0.0	29.1	1.9	23.4	0.0
SO 4138a	363538	1165783	1528	13.4	2899	Gedamawit	CS	21.51	0.60	21.56	0.62	0.84	0.40	0.08	0.40	32.68	3.82	33.3	2.9	13.8	0.0	6.1	1.0	40.0	3.0
SO 4137	363595	1165789	1528	13.4	2909	Gedamawit	CS	17.52	0.64	17.09	1.21	1.14	0.43	0.22	0.60	38.62	3.34	23.9	23.2	20.5	0.0	5.3	0.2	24.9	1.9
SO 4135	363122	1165990	1513	13.7	2183	Gedamawit	CS	21.73	0.66	20.41	1.02	0.99	0.42	0.14	0.53	37.69	3.64	28.8	5.5	17.7	0.0	13.6	0.9	31.2	2.4
SO 4134	345110	1145087	1347	17.4	2183	Gedamawit	CS	21.11	0.88	15.90	0.87	1.01	0.34	0.15	0.44	37.17	2.68	23.2	9.5	15.9	0.0	19.6	3.0	23.6	5.1
SO 4133	363595	1165789	1528	13.4	2940	Gedamawit	CS	22.57	0.34	15.04	1.30	0.79	0.30	0.08	0.28	42.24	2.43	24.8	10.3	16.4	0.0	21.0	1.4	23.3	2.9
SO 4132	362640	1165626	1513	13.7	2940	Gedamawit	CS	17.17	1.02	12.77	1.56	1.24	0.35	0.24	1.15	40.27	2.22	20.8	10.2	15.2	0.0	7.2	0.3	36.0	10.2
SO 4120	362600	1165600	1513	13.7	2940	Gedamawit	CS	22.59	0.31	15.10	1.28	0.78	0.31	0.07	0.29	42.49	2.44	25.0	10.2	11.9	0.0	22.9	1.4	28.5	0.0
SO 4117	362600	1165600	1513	13.7	2940	Gedamawit	CS	23.45	0.32	15.76	1.33	0.82	0.31	0.07	0.30	43.32	2.56	17.7	8.1	17.3	0.0	22.1	1.3	20.2	3.3
SO 4115	362600	1165600	1513	13.7	2940	Gedamawit	CS	22.27	0.31	14.96	1.27	0.79	0.32	0.08	0.29	41.77	2.42	25.6	12.5	16.6	0.0	23.6	1.5	20.4	0.0
SO 4112	362703	1165693	1513	13.7	2940	Gedamawit	CS	19.79	0.72	16.39	1.08	1.12	0.54	0.26	bdl	39.67	2.43	23.8	13.1	16.0	0.0	8.9	0.5	34.4	3.3
SO 4111	362643	1165629	1513	13.7	2940	Gedamawit	CS	17.59	1.08	12.86	1.59	1.28	0.36	0.25	1.15	41.19	2.30	17.9	44.9	13.6	0.0	5.1	0.3	15.1	3.1
SO 4110b	362649	1165626	1513	13.7	2940	Gedamawit	CS	19.37	0.66	15.90	1.03	1.11	0.47	0.27	1.48	39.71	2.42	21.8	8.7	21.4	0.0	7.4	0.3	34.6	5.8
SO 4110a	362649	1165626	1513	13.7	2940	Gedamawit	CS	17.94	1.12	13.21	1.65	1.32	0.36	0.25	1.15	42.02	2.33	20.5	9.3	19.5	0.0	10.6	0.6	32.4	7.1
SO 4107	363444	1165833	1528	13.4	2940	Gedamawit	CS	20.23	0.61	19.43	0.74	0.92	0.41	0.14	0.71	34.18	3.41	25.4	16.7	16.4	0.0	15.7	0.9	24.9	0.0
SO 4106	363444	1165833	1528	13.4	2940	Gedamawit	CS	18.02	0.37	13.42	1.45	1.18	0.30	0.24	0.41	43.67	2.29	19.3	11.8	14.7	0.0	13.2	0.4	32.6	8.1
SO 4105	363451	1165786	1528	13.4	2919	Gedamawit	CS	21.37	0.44	21.74	0.36	0.83	0.37	0.06	0.39	30.89	3.88	36.0	0.0	19.9	0.0	35.4	1.7	7.1	0.0
SO 4104	363795	1166008	1528	13.4	2957	Gedamawit	CS	18.43	0.37	20.26	0.65	0.96	0.47	0.14	0.43	34.23	3.91	29.8	8.1	13.0	0.0	28.4	5.5	10.8	4.4
SO 4098	362710	1166121	1513	13.7	2933	Gedamawit	CS	23.72	0.68	16.73	0.59	0.74	0.29	0.09	0.57	35.57	3.00	32.2	3.0	24.2	0.0	29.4	1.4	9.7	0.0
SO 4097	362939	1166173	1513	13.7	2933	Gedamawit	CS	21.01	0.69	16.53	0.87	0.83	0.36	0.13	0.51	36.91	2.90	25.3	18.0	16.4	0.0	16.3	0.7	20.6	2.8
SO 4036	341014	1165576	1528	13.4	2933	Gedamawit	CS	16.09	0.64	13.49	1.49	1.31	0.33	0.35	0.98	44.93	2.61	18.6	11.4	14.5	14.4	7.2	0.2	25.9	7.8
SO 4024	365524	1165798	1531	13.2	2942	Gedamawit	CS	19.26	0.35	13.78	1.45	1.11	0.28	0.20	0.44	46.67	2.49	21.5	11.1	15.4	0.0	21.4	1.0	25.5	4.2
SO 4022	365144	1165743	1531	13.2	2939	Gedamawit	CS	16.72	0.41	13.79	1.51	1.24	0.32	0.32	0.74	48.34	2.57	19.1	15.5	14.6	0.0	12.7	0.5	31.4	6.1
SO 4020	341012	1120110	1531	13.2	2262	Gedamawit	CS	22.10	0.60	21.79	0.51	1.00	0.35	0.12	0.53	34.53	3.90	30.9	5.7	18.3	0.0	30.5	3.3	11.3	0.0
SO 4003	365444	1165833	1531	13.2	2941	Gedamawit	CS	15.90	0.92	13.39	1.57	1.11	0.36	0.30	0.79	40.61	2.65	20.0	10.8	14.9	14.9	10.1	0.5	25.6	3.2

Note: Multiple sampling at one location are indicated with a letter after the sample number (e.g., 2A and 2D).

to 0.05 to represent the maximum potential error in XRD quantitative measurements. The IBM SPSS statistics program (versions 20 and 21) was used for the PCA calculations. The data from the PCA were used to create a ternary plot (using the 3-axis rule of Tolosana-Delgado et al. 2005) that identifies and distinguishes the geochemical variations in the parent rock, in addition to the extent of weathering.

The degree to which the soils were influenced by the parent rock was also investigated by comparing the chemistry, mineralogy, and derived-weathering indices of the soils collected over the two parent rocks: the Mt. Choke shield basalts and surrounding flood basalt, using a non-parametric Mann-Whitney-U test.

Normative mineralogical data for the unweathered parent rock samples collected on Mt. Choke and the CRMs were not available, and therefore whole rock mineralogy was determined using Cross, Iddings, Pirsson, and Washington (CIPW) norm calculations (Kelsey 1965; Johannsen 1931; Cross et al. 1902). CIPW norm calculations work on the basis that a defined set of minerals (mode) within volcanic rocks can be used to quantitatively estimate the mineralogical composition based on total elemental analysis and defined mineral formulas (Appendix Table 1[1]). The samples used for the CIPW norm calculations, were considered to be fresh or had only minor alteration.

Results

Climate

There was a negative correlation between MAP and MAT ($r = -0.85$, $p = 0.00$; Appendix Table 2[1]). On average MAP in the sample sites was 1446.5 mm/yr, and MAT was 15.3 °C. Elevation correlated negatively with MAT ($r = -0.82$) and positively with MAP ($r = 0.83$).

Soil chemistry

The values for the major element chemical analyses and quantification of the mineral phases within the soil are shown in Table 1, and Spearman's Rank correlations between the data are shown in Appendix Table 2[1]. Strong correlations (where $r \geq 0.5$ and $p \leq 0.01$) involving wt% Fe_2O_3 were observed, negatively with SiO_2 and K_2O ($r = -0.71$ and -0.82, respectively) and positively with TiO_2 ($r = 0.77$). In addition, Na_2O_3 correlates negatively with Al_2O_3 ($r = -0.82$) and positively with MgO ($r = 0.53$), while K_2O correlates negatively with TiO_2 ($r = -0.66$) and positively with SiO_2 ($r = 0.71$). Finally, SiO_2 correlates negatively with TiO_2 ($r = -0.62$). The correlations observed in the surface soils approximately reflect the chemical characteristics of the volcanic parent rock, where the proportion of elements more commonly found in mafic rocks (Fe, Mg, Ca, Ti) were generally negatively correlated with those found in more felsic rocks (Si, Na, K).

SiO_2 negatively correlated with MAP ($r = -0.52$) and MgO negatively correlated with MAT ($r = -0.656$) (Appendix Table 2[1]). No other bulk oxide was found to have a strong correlation (where $r \geq 0.5$) with either temperature or precipitation (MAT or MAP).

The data from the characterization of the soil samples were grouped according to the parent rock (i.e., Mt. Choke shield volcano and flood basalt). A non-parametric Mann-Whitney U test was used to determine whether the two sets of data were significantly different (where $p < 0.05$). The outcomes of the statistical analysis are detailed in Table 2, which shows that the soils formed on the Mt. Choke shield volcano were significantly different in their chemistry (for all elements) compared with those formed on the flood basalt.

Soil mineralogy

The soils were generally iron-oxyhydroxide-rich (goethite; 16–40 wt%; Table 1), with varying proportions of amorphous silica (9–26 wt%; indicated by the characteristic XRD pattern showing a "hump" centered at ~21 °2θ; e.g., Fig. 2a), quartz (0–45 wt%), feldspars (either in concentrations 11–30 wt% or completely absent) and phyllosilicates (totaling 9–57 wt%). Other minor phases were occasionally observed in the XRD identification, for example pyroxene was observed and some minor crystalline iron oxide phases (e.g., hematite; Fig. 2b), but at levels <<5 wt%, and hence they were not included in the quantification. The phyllosilicates included mica, chlorite, kaolinite, and kaolinite-smectite (K-S), the latter with either high smectite (50 to 70%) or high kaolinite (95 to 97%) contents. The high smectite K-S was detected in the diffraction patterns of the oriented mounts, where the air-dry samples displayed a broad peak at 14.3 Å that was displaced after glycolation to 17.4 Å (Fig. 2c).

The 060 peak is broad and centered ~1.49–1.50 Å (Fig. 2b) confirming that the kaolinite and K-S were dioctahedral (octahedral cation abundance is Al >> Fe, Mg). The broad 060 peak may also mask the mica (dioctahedral) peak at 1.50 Å (similarly the quartz peak at 1.54 Å overlies and hides the influence of the chlorites (at ~1.53–1.55 Å).

The K-S phases were divided into their kaolinite and smectite components to produce an overall quantity of each layer type within the soil. For example, the amount of kaolinite is the sum of the percentage of the discrete kaolinite plus the proportion of kaolinite layers in the K-S (mixed-layer) phases. Figure 2d provides an example of match between a calculated and experimental XRD pattern of an oriented, glycolated mount preparation. The 001 peak of the calculated XRD pattern is displaced to a lower angle due to the combined effect of the low intensity of the peak and the steep background (Fig. 2d). The ClaySIM program, used in the quantification of the phyllosilicates, typically produces a steeper pattern background than the experimental pattern in the low-angle region (Plançon 2002). The simulations, however, rely

Table 2. Summary statistics of the data (chemical composition, mineralogy, and weathering indices) to test for significant differences between the samples of soil over the Mt Choke shield deposits and the flood basalts using a non-parametric Mann-Whitney U test

	Significant difference between Choke shield and flood basalts?	Significance (p)	Test statistics (Z)
	Chemical composition (wt%)[a]		
Al_2O_3	YES	0.00	11.7
CaO	YES	0.00	10.1
Fe_2O_3	YES	0.00	10.2
K_2O	YES	0.04	4.1
MgO	YES	0.00	35.8
MnO	YES	0.00	8.9
Na_2O_3	YES	0.00	12.3
P_2O_5	YES	0.00	38.7
SiO_2	YES	0.00	38.9
TiO_2	YES	0.00	16.5
	Mineralogy (%)[b]		
Fe oxide	YES	0.02	5.7
Quartz	YES	0.01	6.4
Amorphous silica	YES	0.00	11.4
Feldspars	NO	0.30	1.2
Kaolinite	YES	0.02	5.8
Smectite	NO	0.52	0.4
Mica	NO	0.78	0.1
Chlorite	YES	0.00	33.8
	Indices of weathering		
CIA[a]	NO	0.86	3.0
CIW[a]	YES	0.00	15.4
W index[a]	YES	0.00	11.4
W_{min} index[b]	YES	0.00	19.0

[a] Choke shield $n = 51$, Flood basalt $n = 82$. [b] Choke shield $n = 40$, Flood basalt $n = 60$.

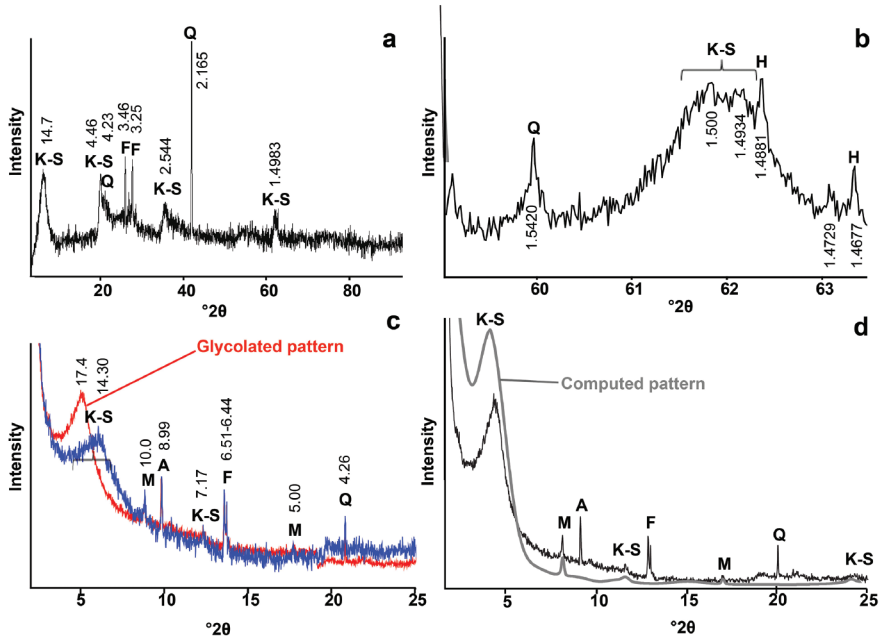

FIGURE 2. XRD patterns for the soil sample DM-CM SO 26A (with *d*-spacings written vertically, in angstroms), (**a**) bulk soil side-loaded mount, (**b**) limited °2θ range to show the 060 peaks of the clays within the samples, (**c**) air-dried and glycolated versions of the oriented mount preparation, and (**d**) clay modeling of the glycolated, oriented mount. A = amphibole, F = feldspars, H = hematite, K-S = kaolinite-smectite mixed-layer clay, M = mica, Q = quartz. NB the major quartz peak in a is likely due to a single large crystal in the powder.

on the position of all 00*l* peaks in the experimental patterns and the calculated pattern in Figure 2d can be considered to be a true representation of the experimental pattern.

Significant negative correlations were observed in the soils between the quantity of quartz and amorphous silica ($r = -0.54$; Appendix Table 2[1]). A negative correlation between the amount of mica and kaolinite ($r = -0.61$) was also noted. Chlorite was found to positively correlate with both MAP and MAT (Appendix Table 2[1]). No other mineral phase was found to have a strong correlation (where $r \geq 0.5$) with either MAT or MAP.

The specific alteration products of some of the most abundant minerals in the original rock and the potential mechanisms of clay formation were further investigated using SEM. Specifically, two issues were explored: first, the alteration process by which kaolinite phases were formed; second, the form of the amorphous silica within the soil. For the SEM work, two soil samples (SO 5137 and DM-CM SO 7A) with high quantities of kaolinite and amorphous silica were fixed in resin and polished. Kaolinite was observed as an alteration product of both feldspars and perhaps quartz, forming distinct weathering rims. An example of a quartz grain is shown in Figure 3, where the outer rim of the quartz grain has been transformed into kaolinite. The similarities between the shapes of the grain and the coating also point to this theory of transformation rather than an inherited coating, however, more work is need to confirm this. Kaolinite-rich phases were ubiquitous within the soil samples analyzed by SEM-EDS, but in most cases the K-S was found in the soil matrix and there was no preserved relation to the original mineral grains. In addition, no discrete regions of pure amorphous silica were observed in the resin soil blocks under the SEM (with EDS). It is therefore surmised that the amorphous silica must occur as fine groundmass (intergrown with clay minerals and Fe oxides) in the soil, which is in agreement with other studies (e.g., Singh and Gilkes 1993).

In terms of the soil mineralogy over the two different parent rocks, the quantity of iron oxides, quartz, amorphous silica, kaolinite, and chlorite was significantly different in soils over the flood basalt when compared with the Mt. Choke shield (Table 2). However, the content of feldspars, smectite, and mica measured in the soils were not significantly different over the two parent rocks.

Multivariate regression analysis was used to investigate associations between bulk chemical composition of the soils and their mineralogical phases ($r \geq 0.5$, $p \leq 0.01$ was considered significant). The most significant relationship was observed between the Fe_2O_3 concentration and quantities of FeOOH, mica, and chlorite from XRD quantification ($R^2 = 0.754$, $R^2_{adjusted} = 0.746$):

$$\text{wt\% } Fe_2O_3 = 3.235 - (0.021 \times \text{wt\% mica}) + (0.077 \times \text{wt\% chlorite}) + (0.529 \times \text{wt\% Fe oxide}) \quad (1)$$

Geochemical weathering indices

The CIA values for the soil samples varied in the range 68.4–96.7 ($n = 135$, average = 87.4), and the CIW values were 78.7–98.5 ($n = 135$, average = 93.1) (not shown). The average CIA and CIW values calculated for the unweathered parent rock were 40.8 and 41.8, respectively. The average CIA and CIW values calculated for the CRMs were 37.2 and 39.8, respectively.

The CIA and CIW values correlated positively ($r = 0.75$; Appendix Table 2[1]), and the CIA correlated positively with kaolinite ($r = 0.52$) and iron oxide ($r = 0.59$). Both CIA and CIW correlated positively with Al_2O_3 and Fe_2O_3, and negatively with Ca-, Na-, and K-oxides.

The *W* index calculations (derived from Ohta and Arai 2007) were plotted onto a ternary diagram, to represent the three latent variables: mafic source, felsic source and relative extent of weathering (shown as the three vertices M-F-*W* on the ternary plot in Fig. 4). The majority of the soil samples concentrate in the region of the M-F-*W* plot that indicates high weathering, derived from basaltic rocks. The parent rocks and CRMs plot between the M-F vertices, the solid arc on which they plot indicating no alteration. The unweathered parent rock, however, show that there is varia-

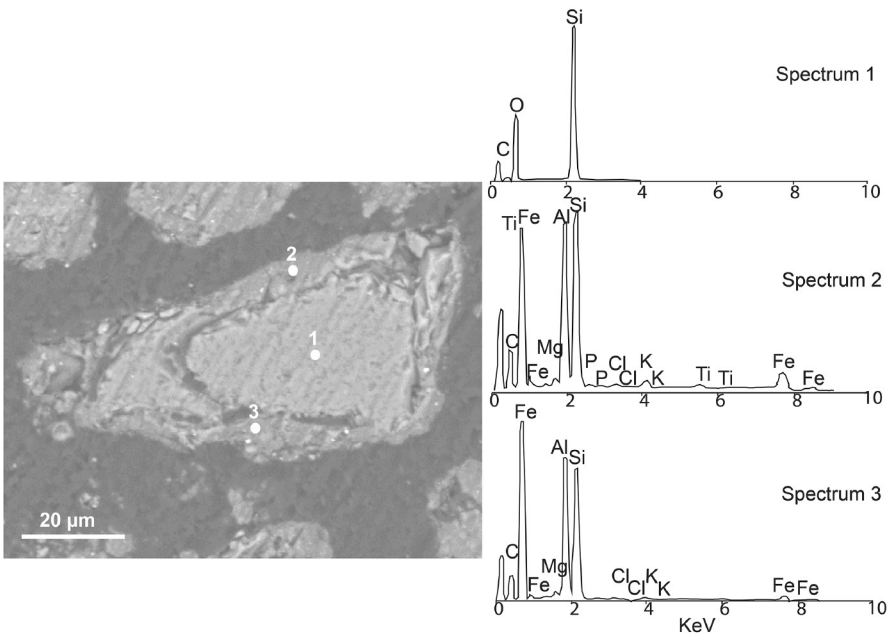

FIGURE 3. SEM (BSE) image of a quartz grain with a rim of kaolinite generated by weathering, from soil sample SO 5137. The spots on the BSE image represent the locations of the EDS spectra: spectrum 1 = quartz; spectra 2 and 3 = kaolinite.

tion in the chemistry of the samples collected from the flood basalt and Mt. Choke regions. The soils collected above the Kutye basalt deposit (near the summit of Mt. Choke shield) plot relatively closer to the "F" vertex, however, the majority of the soil samples are clustered together and it is challenging to resolve the detail in the mass of points at the "*W*" apex.

Deriving the W_{min} index

PCA of the mineralogy data (Table 3) suggests that the first principal component (PC1) is positively correlated with the amorphous silica, kaolinite, amorphous iron oxides, mica, and smectite, and negatively with feldspars, crystalline iron oxide, pyroxene, and olivine. The second principal component (PC2) shows a strong positive correlation with chlorite, a weak negative relationship with olivine, and also a weak but positive correlation with quartz. PC1 and PC2 represent 70.1 and 13.7% of the variance (respectively) and collectively the three components explain 84.8% of the variance within the samples. The resultant biplot using PC1 and PC2 (e.g., Aitchison and Greenacre 2002) is shown in Figure 5. The values for the individual soils are plotted as discrete points on the biplot, and the "mineral" phase loadings are represented by the arrows radiating from the central point of the biplot (representing the PCA loading scores in Table 3). The mineral phases (variables) are represented in this bi-plot by a vector, and the direction and length of the vector indicate how each variable contributes to the two principal components in the plot. Values for the mineralogy of the CRMs and unweathered parent rock (Appendix Table 1[1]) are from CIPW norm calculations, and are plotted on the biplot,

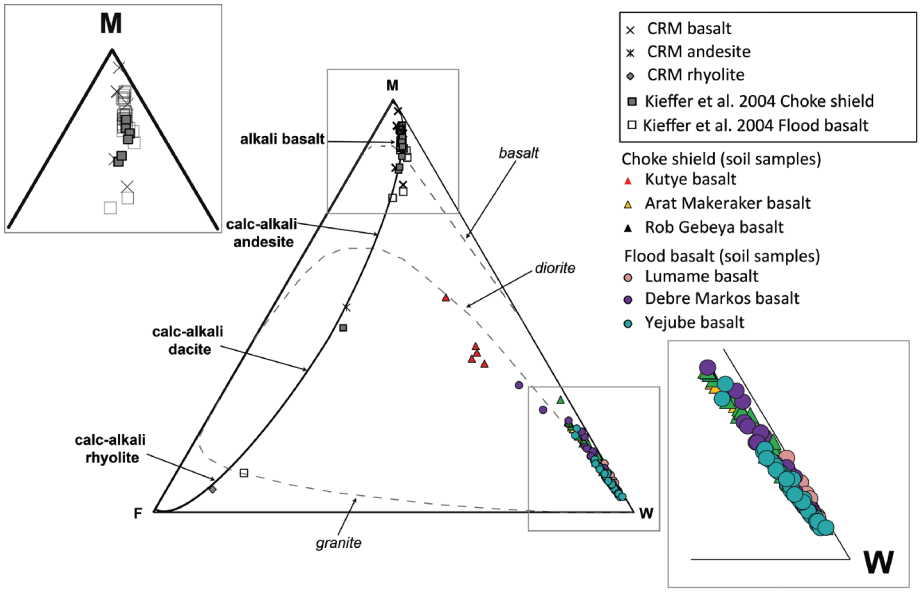

FIGURE 4. Ternary M-F-*W* plot showing the degree of weathering with the soils (n = 135) (adapted from Ohta and Arai 2007 and references therein). The vertices correspond to pristine mafic (M) and felsic (F) rocks, and the completely weathered material (*W*). The curved, solid line indicates the location of pristine rock of intermediate mafic-felsic composition and the dashed lines represent the pathways of the composition from the original rock to a completely weathered material (details in Ohta and Arai 2007).

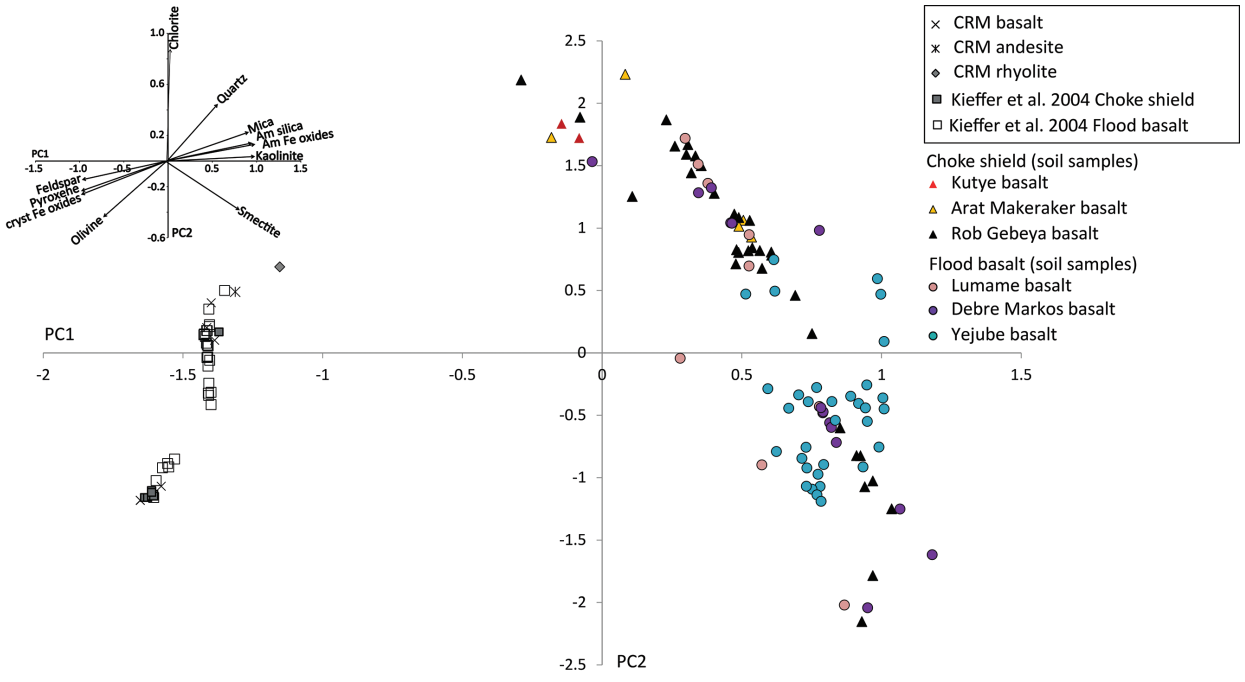

FIGURE 5. Principal component analysis (PCA) of the mineralogy of the soil samples (n = 100), and calculated mineralogy of pristine samples of the unweathered parent rocks (from Kieffer et al. 2004) and CRMs. The loadings of each of the mineral phases are given by the arrows in the top left.

in addition to the soil samples, for comparison. The unweathered parent rocks and CRM samples have negative PC1 scores (Fig. 5), whereas the soil samples have comparatively more positive PC1 scores. There is also separation of the samples according to the PC2 scores, from those samples that are smectite-rich (with negative PC2 scores), to those that are quartz and/or chlorite-rich (with positive PC2 scores).

The orthogonal components (calculated from PCA), representing the main controls on the mineralogy of the soils (PC1 and PC2, Fig. 5), were reformatted to plot on a ternary diagram using Equation 2 (see Ohta and Arai 2007, for further details):

TABLE 3. Results of the principal component analysis (PCA) of the soil mineralogy, including the total variance, loadings, and component scores calculated from the mineralogy

	PC1	PC2
Initial Eigenvalues (Total)	7.81	1.52
Cumulative (%)	70.98	84.77
Loadings for each mineral		
amorphous Fe oxide	**0.977**	0.130
crystalline Fe oxide	**–0.946**	–0.263
quartz	0.570	0.442
feldspars	**–0.936**	–0.142
kaolinite	**0.976**	0.029
smectite	**0.805**	–0.380
mica	**0.909**	0.220
chlorite	0.038	**0.868**
pyroxene	**–0.946**	–0.244
olivine	**–0.700**	–0.435
amorphous silica	**0.973**	0.136

Notes: The Eigenvalues for the components 1–3 were >1. Varimax Rotation (converged in three iterations) was used to calculate the Cumulative % loading. The loadings were calculated for each of the mineral phases for the first 2 components. Bold values (where loadings are >0.6) are considered significant (e.g., Kirkup 2012).

$$V_1 = \exp\left(\frac{-1}{\sqrt{6}}PC1 + \frac{-1}{\sqrt{2}}PC2\right), V_2 = \exp\left(\frac{-1}{\sqrt{6}}PC1 + \frac{-1}{\sqrt{2}}PC2\right), V_3 = \exp\left(\frac{2}{\sqrt{6}}PC1\right) \quad (2)$$

Then, V_1, V_2, and V_3 were normalized and used to create the "mafic", "felsic," and "W_{min}" vertices in the ternary diagram (Fig. 6a). The unweathered parent rock and CRMs, plot along a line delimiting the furthest distance from the "W_{min}" apex on the ternary diagram, next to the mafic-felsic joining line (Fig. 6a). In a similar way to the W index, the parent rock samples plot along the range of mineralogy delimiting felsic and mafic samples accordingly. The soil samples collected in this study plot as an arc progressing away from the felsic-mafic axis toward the "W_{min}" apex (Fig. 6a). The extent of weathering within the soils is shown by the variable distance between the "W_{min}" apex and the datapoints. It is worth noting that the scales on the ternary diagrams used to represent the W (Fig. 4) and W_{min} (Fig. 6a) indices do not represent a complete scale from 0 to 100%, but are specific to the compositional and weathering ranges included in the analysis.

The W_{min} index correlates positively with MAT (r = 0.57), and negatively with both MAP and elevation (r = –0.5 and r = –0.58, respectively; Appendix Table 2[1]).

DISCUSSION

Soil formation

Pedogenesis occurs over time to alter the chemistry and mineralogy of the parent rock to create soils that contain mineral phases considered stable at the Earth's surface. The surface soils characterized in this investigation were composed of minerals

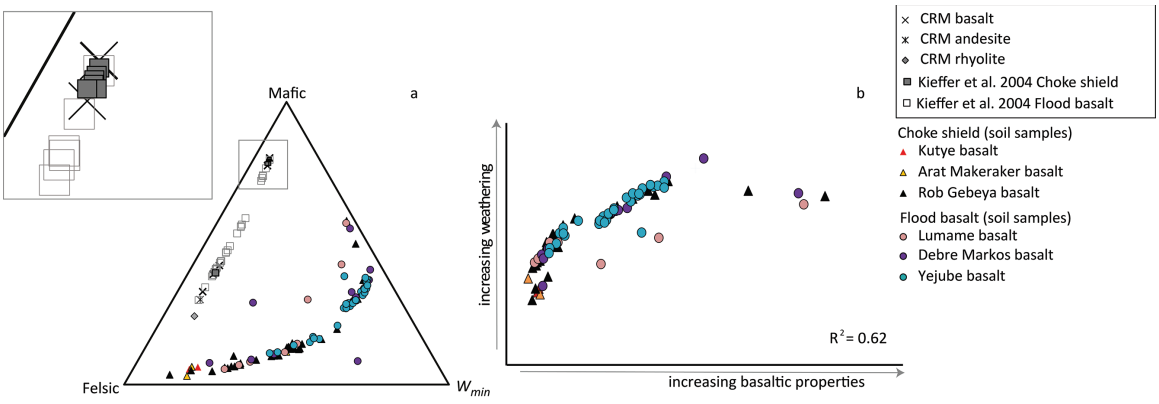

FIGURE 6. (**a**) W_{min} ternary plot to show the extent of weathering within the soil samples calculated from mineralogy (n = 100), including the unweathered parent rock samples underlying the soils in our study (Kieffer et al. 2004) and CRMs (where the mineralogy was determined by CIPW norm calculations). (**b**) Correlation between the extent of weathering and felsic mineralogy of the soil samples.

that typically result from the alteration of basaltic rock over time, such as iron oxides, phyllosilicates, and amorphous silica. During weathering, the most mobile elements (Mg, Ca, Na, and K) become depleted via various processes including congruent and incongruent dissolutions, oxidation, and hydration reactions. The mechanisms occurring during weathering that alter the primary minerals to secondary minerals may be either sub-solidus replacement or dissolution-precipitation, and can form either crystalline structures or non-crystalline phases (e.g., Viti et al. 2007). The breakdown of the primary minerals in our soil samples (pyroxene, olivine, feldspars) and volcanic glass has resulted in the loss of non-hydrolyzing cations (at least Ca^{2+}, Na^{+}) and the accumulation of Si^{4+}, Al^{3+}, and Fe^{3+} cations preserved in crystalline (e.g., kaolinite) and amorphous/poorly crystalline phases (e.g., FeOOH). Hence, with increasing weathering the total amount of phyllosilicates and proportion of Fe oxides increases within the soil (Delvaux et al. 1989).

Kaolinite and mixed-layer K-S clays were present in most of our soil samples. These minerals have been found to be a common constituent in soils with a basaltic parent rock across tropical, subtropical, and semi-arid regions (Vingiani et al. 2004; Righi et al. 1999; Delvaux et al. 1990). Primary minerals in igneous rocks eventually weather to clay minerals (Taylor and McLennan 1985; Taylor et al. 1983) and in regions with high annual precipitation, as in our study area, kaolinite is typically the final product of weathering. The soils analyzed in our study contained both a proportion of discrete kaolinite and K-S that was either kaolinite-rich (with 95 to 97% kaolinite layers) or smectite-rich (with 50 to 70% smectite layers). No K-S mixed-layer phases were found with intermediate kaolinite contents (i.e., between 50 and 94%). As smectite transforms into kaolinite in highly weathered soil environments, one would expect to find the entire range of K-S compositions present in our soils (e.g., Herbillon et al. 1981). Our modeling procedure does not totally exclude the existence of K-S of "intermediate" composition; however, if this phase is present, it is in much lower concentrations (relative to pure kaolinite, or kaolinite- and smectite-rich K-S forms). We conclude that this gap in K-S composition indicates a degree of alteration heterogeneity within the soils that needs to be explored further.

The multivariate analysis, comparing the soil mineralogy with the bulk chemistry, indicated that the majority of the iron in the soils is held within the amorphous/poorly crystalline iron oxide phases. There was also a positive correlation with chlorite indicating that the chlorite contains iron. The negative correlation of the mica in the regression equation implies that the mica must be in a form that is Al rich and Fe poor. When kaolinite and smectite were included in the regression analysis (Eq. 2), their contributions to the R^2 value were insignificant. We recall that the kaolinite and smectite included the proportion of layers in K-S as well as end-member kaolinite; i.e., smectite and kaolinite indicates layers in K-S to a large extent. The lack of correlation between kaolinite and iron was surprising, because one would have expected a significant negative correlation between them. Our interpretations are that both smectite and kaolinite layers contain iron and that the quantity of iron in these clays must be approximately proportional to the iron in the glass and primary minerals from which they formed. Hence, no correlation emerged between these minerals and iron content. The incorporation of iron into smectite, at variable proportions, is well known; however, it is more difficult to justify the presence of iron in kaolinite. Nonetheless, the presence of iron was confirmed within kaolinite, as SEM-EDS analysis consistently showed iron within the spectra of kaolinitic grains (e.g., Fig. 3). The incorporation of Fe^{3+} ions into the octahedral sites of kaolinite has previously been documented (Weaver et al. 1967; Malden and Meads 1967), and Iriarte et al. (2005) synthesized kaolinite with up to ~⅓ of octahedral sites occupied by iron ($Si_2Al_{1.4}Fe_{0.6}O_5[OH]_4$). In addition, in our soil samples the majority of the kaolinite was found in a mixed-layered (K-S) form, where kaolinite layers have been shown to incorporate significant amounts of iron (Dudek et al. 2006; Ryan and Huertas 2009).

We propose that the kaolinite- and smectite-rich K-S phases are the products of alteration from different mineral phases in the parent rock. More specifically, feldspar would alter into kaolinite and kaolinite-rich K-S, while volcanic glass and perhaps additionally olivine and pyroxene, would alter to smectite (which would subsequently alter to K-S of progressively kaolinitic composition). These processes were compatible with our SEM observations. In this study, kaolinite and kaolinite-rich K-S was observed surrounding grains of feldspar and less frequently, but notably,

around quartz (Fig. 3), in what appeared to be alteration rims. This observation is of interest because, in systems similar to this, smectite is perceived to be an intermediate stage of weathering toward K-S that ends in the formation of kaolinite. However, our observations suggest that K-S can also form without a smectite precursor. The alteration of quartz to kaolinite (or kaolinite-rich K-S) may be made possible by the direct contact with other mineral grains containing Al, also in the process of weathering or dissolution. The smectite-rich K-S was predominantly found in the soil matrix and without spatial or morphological reference to original primary minerals (i.e., relic features) and hence may indicate that smectite-rich K-S formed mainly from the alteration of volcanic glass in the parent rock matrix.

Weathering indices

Weathering indices are conventionally used to quantify the extent of weathering within a sample soil (or other unconsolidated sediment or rock) and help to explain processes occurring during pedogenesis. CIA values calculated for pristine basalts collected on the Deccan Traps in India were ~35 (Babechuk et al. 2014), whereas the CIA values for residual clays lie between 85 and 100 (Taylor and McLennan 1985) and pure kaolinite approaches 100 (Nesbitt and Young 1982). The CIW values calculated for pristine basalts collected in Iceland were between 37 and 38, and andosol soils (developed over volcanic rock) ranged from 37–45 for weakly weathered soils to 50–77 for more strongly weathered soils (Óskarsson et al. 2012). Similarly, CIW values for strongly weathered volcanic soils (laterites) developing in warmer climates in Brazil and China have been calculated to be between 70 and 100 (e.g., Ma et al. 2007; Truckenbrodt et al. 1991). The CIA and CIW values calculated in this study reveal that the extent of weathering within the soil samples is relatively high (CIA average = 90.5, CIW average = 96.1). The unweathered parent rock samples and the CRMs had significantly lower values for CIA and CIW, of <42, which indicated that they effectively represent the unaltered, parent rock.

The ternary diagram for the *W* index shows the chemical composition of the parent rock samples, relative to the soil samples (Fig. 4). The CRMs plotted as expected, with the rhyolite RGM-1 (Appendix Table 1[1]), plotting near the "F" (felsic) axis, the basaltic samples plotting near the "M" (mafic axis) and the andesite AGV-1 midway between the "F" and "M" axis. The unweathered parent rocks, however, have varied compositions: Almost all of the rock samples collected on the flood basalt plot near the "M" axis, with the exception of sample 139, which plots near to the "F" axis. However, this sample was classified as "trachyte" and was recognized as being more felsic than the other samples from the flood basalt deposits. The majority of the parent rock samples collected on the Mt. Choke shield were classified as "basalts" and plot accordingly near to the "M" axis on the ternary diagram, with the exception of sample 240. This sample was identified as a "trachyandesite" and plots accordingly on the ternary plot, indicating that there is a distinct felsic character to the deposits on the upper elevations of Mt. Choke. The chemical characteristics of the soil reflect that there may be an influence by the felsic parent rock because the soils collected on the Kutye basalt at the summit of Mt. Choke (~3700 m) plot relatively closer to the "F" axis. In addition, these soils from the summit of Mt. Choke appear to be less weathered (i.e., further from the "W" axis) when compared with the other soil samples.

Information from the W_{min} index

The biplot calculated for the W_{min} index (Fig. 5) suggests that PC1 corresponds to the degree of weathering, which was defined as the amount of feldspars, crystalline iron oxide, pyroxene, and olivine, vs. the amount of amorphous silica, amorphous iron oxide and phyllosilicates within the sample. This is exemplified by the placement of the parent rock samples relative to the soil samples along the PC1 axis. Mica is not expected to be a weathering product but perhaps its resistance to weathering makes it more concentrated in the soils and thus positively correlated with weathering. One other, alternative, explanation for the positive correlation with weathering is that here we did not differentiate between mica and illite (the latter being a product of weathering in soils).

Chlorite had a strong positive loading on the PC2 axis and quartz a weaker positive loading. Olivine, and to a lesser extent smectite, had a moderate negative loading on the PC2 axis. Chlorite is a group of phyllosilicates that can be formed by hydrothermal alteration of igneous rocks and the alteration of ferromagnesian minerals (Meunier 2005). Chlorite was present in all the soil samples collected on the Kutye and Arat Makeraker basalts deposit, had a negative correlation with elevation, but was only sporadically present in the soils collected at lower elevations. In addition, the amount of chlorite was also negatively associated with MAT and positively correlated with MAP.

When considering the placement of olivine and quartz, the PC2 axis is likely to represent the chemistry of the parent rock composition, with a mafic to felsic transition from negative to positive PC2 values. If the unweathered parent rocks are taken as an example, negatively loaded PC2 samples have increased amounts of olivine and are from a more mafic rock, whereas positively loaded PC2 samples have more quartz and are more felsic. It must be recognized, however, that PC2 does not represent a completely regular scale from mafic to felsic, as the more mafic parent rocks extend from PC2 = –2.5 to 0.5, and the felsic samples plot in the range = >0.5. The very high loading of chlorite in PC2 may be related to chemistry (Al-rich) or to the higher efficiency of the more felsic magma in producing chlorite because of the higher water content. The soils showed a wide degree of separation, particularly between those collected on the Kutye and Arat Makeraker basalts and the Yejube basalt deposits. The soils collected on the Rob Gebaya, Lumame, and Debre Markos basalts, however spanned the range of the PC2 axis, which is representative of the wide variation in parent rock composition. The degree to which the soils have been weathered (calculated as "W_{min}") was correlated with the increase in mafic mineralogy of the soil (Fig. 6b), and W_{min} correlated positively with the amount of smectite (r = 0.55).

Although the PCA has differentiated the samples according to both the extent of weathering and the nature of the unweathered parent rock, we must consider that mineralogy of the parent rocks was derived from CIPW norm calculations and not actual measurements (for example quantification by XRD). It must be

acknowledged that the CIPW norm calculations have a distinct error when used in this context, as the volcanic glass likely present in the unweathered parent rock matrix is not accounted for. This would influence the amorphous silica content, and potentially reduce the loading in the positive region on the PC1 axis. Mineral phases quantified by the CIPW norm calculations, for example pyroxene and crystalline Fe oxide phases, were observed in the SEM and XRD analysis (respectively) of the soil samples. Hence, the mineral phases predicted by CIPW are likely to be present in the original parent rock and thus the CIPW norm calculations have provided a good estimate of the rock mineralogy. It is also worth noting that the iron oxide derived from the XRD quantification was predominantly in a poorly crystalline form. However, we observed trace (i.e., <<5%) amounts of crystalline iron oxide, hematite, in the XRD patterns of the soil samples (Fig. 2b), that is negligible in the quantification of iron phases that was carried out.

Comparison of weathering indices

In principle, a correlation is expected between the chemical weathering indices and the proportion of secondary minerals formed by weathering. In this study, there was a positive correlation of CIA values with both amorphous Fe oxide (r = 0.59) and kaolinite (r = 0.52) (Appendix Table 2[1]), which are both weathering products. However, no significant correlation existed between either the CIW or *W* index and mineral content.

In addition to the extent of weathering, the *W* and W_{min} index ternary diagrams also discriminated between samples according to the nature of the parent rock from which they originated. There was a good correlation between the extent of weathering and the nature of the parent rock for the soil samples analyzed in this study (r = 0.62, Fig. 6b). Soil samples that were more felsic, in terms of their mineralogy, were comparatively less weathered. This compositional effect on weathering extent can also be observed in the ternary plots (Figs. 4 and 6a). For example, the Kutye basalts were relatively more felsic than the other basalts and the corresponding soils were shown to be comparatively less weathered (Figs. 4 and 6a). This is an expected result because minerals in progressively more felsic rocks, such as quartz and mica, are more resistant to weathering than those typically found in more mafic rocks (pyroxene and amphibole); likewise K-feldspar is more resistant than Na and Ca feldspars (e.g., Retallack 2001; Albarede and Michard 1986; Holland 1984; Edmond et al. 1979). Small chemical differences in magma can result in significantly different mineral components within the parent rock, which impacts the overall resistance to weathering. Hence, a weathering index based on mineralogy, has the advantage over a chemical index that it will more readily reveal the cause of differential weathering linked to mineralogy.

Comparison of the W_{min} and *W* indices shows the following differences. (1) In the *W* index ternary diagram (Fig. 4), the unweathered parent rocks plotted along a concave arc spanning the mafic-felsic apices and extend into the plot, whereas in the W_{min} index diagram (Fig. 5) these same data points plotted next to the straight line joining the mafic-felsic apices. (2) The pathways of weathering denoted on the *W* index diagram (dashed lines, Fig. 4) are not necessarily intuitive and need to be identified for each parent rock type, whereas the weathering pathways in the W_{min} index ternary diagram can be determined by the relative distance from the *W* apex. From these two observations the W_{min} index configuration is more intuitive as the parent rocks are at the furthest distance away from the *W* axis, and soil samples simply plot relative to each other without conforming to a pathway that must be specified. (3) The data points in the *W* index plot are compressed toward the *W* axis, whereas the plotting range is extended on the W_{min} plot. Thus, differences between samples may be lost or masked when using the *W* plot, whereas the W_{min} index ternary diagram may reveal comparatively greater resolution within sample data points.

The *W* and W_{min} weathering indices provide a method of establishing both the degree of weathering, and an indication as to the nature of the parent rock from which the soil sample was formed. The CIA and CIW chemical indices of weathering, when used alone, can provide an estimate of the extent of weathering but details are lost within the complexity of the weathering processes. This is in general agreement with the conclusions from others (e.g., Price and Velbel 2003; Duzgoren-Aydin et al. 2002), who have questioned the validity of using a selective array of elements to explain the complex processes occurring within weathering profiles. Although it is often less time consuming to determine the bulk chemical composition and calculate the *W* index for a suite of samples, we would additionally advocate the use of the W_{min} index.

Implications

The extent of weathering within the soils, and samples within a soil profile, is traditionally quantified by chemical indices based on the relative proportions of common immobile to mobile cations (CIA, CIW). An advancement on these chemical indices is the multivariate statistical analysis of the entire cation suit that has been used to derive the *W* index (detailed in Ohta and Arai 2007), which not only calculates the relative extent of weathering but also uses the data to identify the composition of the parent rock. Relating the surface soil to the parent rock from which it was formed is a valuable addition in understanding the evolution of the soils. Following the multivariate mathematical approach, we derive a new method of using mineralogy to determine the degree of weathering within soils forming over igneous parent rocks and the W_{min} index, which also attempts to identify the nature of the parent rock. In this study, we noted that the soils appear to maintain a weak signature of the composition of the original magmatic rock from which they were formed. We identified the benefits of calculating the W_{min} index and used this index to explain the mineralogical processes that have occurred within the soil profile to create the surface soil over time. Briefly, the W_{min} index data points plotted in a more intuitive manner and with greater resolution than the *W* index. Nonetheless, the *W* index is possibly more accurate, due to the greater limitations of mineral phase quantification and is potentially less time-consuming. However, when the *W* index and W_{min} index are used in conjunction, information on both the geochemical and mineralogical processes that occur during the weathering of an igneous parent rock can be acquired.

To better understand and explain the processes occurring during soil formation over igneous deposits, we advocate the use of multivariate statistical analysis of soil data to compare the relative weathering extent between soil samples. Although there are other factors that will inevitably influence the characteristics

of soils, such as erosion and aeolian deposit, the W and W_{min} indices provide a single value for a surface soil that identifies the comparative extent of weathering, and if quantitative data on soil geochemistry or mineralogy is available, then calculation of the W and W_{min} indices can be carried out retrospectively.

The analysis techniques outlined in this paper can be used on various soil samples, and can therefore provide a protocol that can be employed over wide study areas and on a global scale. The aim is to utilize this methodology for surface soil characterization to rapidly compare properties where there is pre-existing data on the chemistry and mineralogy of the soil. The W and W_{min} indices can be used across other flood basalt provinces as well, to test the sensitivity of the indices in differentiating soils from parent rocks with subtle differences in their mineralogy. An additional suggestion is to utilize this methodology to compare the soils forming over very different igneous deposits (ranging from ultramafic to felsic) to better understand the impact that weathering has over different timescales and the regeneration of soil profiles over time. Single values, obtained from the indices, can be mapped spatially and coupled with other categories of information (for example water flow direction and accumulation, climatic, vegetation, from in situ measurements or remote sensing) to conduct comprehensive studies of soils within different environments and weathering regimes. This has implications for agriculture and mineral prospecting, and can potentially be applied over large land areas.

Acknowledgments

This work was funded by a grant from the Wellcome Trust University Award (No. 091956) held at BSMS. The authors thank E. Humphreys-Williams for help with the ICP-AES data analysis and J. Najorka for XRD advice, both at the NHM, London. Thanks also to M. Riishuus for insightful comments on the manuscript in an earlier form.

References cited

Aitchison, J. (1986) The Statistical Analysis of Compositional Data. Reprinted in 2003. Blackburn Press, Caldwell, New Jersey.

Aitchison, J., and Greenacre, M. (2002) Biplots of compositional data. Journal of the Royal Statistical Society, Series C: Applied Statistics, 51, 375–392.

Albarede, F., and Michard, A. (1986) Transfer of continental Mg, S, O and U to the mantle through hydrothermal alteration of the oceanic-crust. Chemical Geology, 57, 1–15.

Alemayehu, M. (2003) Ethiopia. Country Pasture/Forage Resource Profile, http://www.fao.org/ag/AGP/AGPC/doc/Counprof/Ethiopia/Ethiopia.htm. Accessed November 4, 2013.

Babechuk, M.G., Widdowson, M., and Kamber, B.S. (2014) Quantifying chemical weathering intensity and trace element release from two contrasting basalt profiles, Deccan Traps, India. Chemical Geology, 363, 56–75.

BCEOM (1999) Abay River Basin integrated master plan, main report. Ministry of Water Resources, Addis Ababa, 71–83 pp.

Berner, E.K., and Berner, R.A. (1996) Global environment: Water, air, and geochemical cycles. Prentice-Hall, New Jersey.

Bewket, W., and Teferi, E. (2009) Assessment of soil erosion hazard and prioritisation for treatment at the watershed level: Case study in the Chemoga watershed, Blue Nile Basin, Ethiopia. Land Degradation and Development, 20, 609–622.

Chorover, J., Amistadi, M.K., and Chadwick, O.A. (2004) Surface charge evolution of mineral-organic complexes during pedogenesis in Hawaiian basalt. Geochimica et Cosmochimica Acta, 68(23), 4859–4876.

Coulié E., Quidelleur, X., Gillot P.-Y., Courtillot, V., Lefèvre J.-C., and Chiesa, S. (2003) Comparative K-Ar and Ar/Ar dating of Ethiopian and Yemenite Oligocene volcanism: Implications for timing and duration of the Ethiopian Traps. Earth and Planetary Science Letters, 206, 477–492.

Cressey, G. (1999) Recording X-ray snapshots of reaction kinetics: Clay hydration and cation exchange, Microsource Application Note No. 8, http://www.microsource.co.uk, accessed: December 2013.

Cressey, G., and Schofield, P.F. (1996) Rapid whole-pattern profile stripping method for the quantification of multiphase samples. Powder Diffraction, 11, 35–39.

Cross, W., Iddings, J.P., Pirrson, L.V., and Washington, H.S. (1902) A quantitative chemico-mineralogical classification and nomenclature of igneous rocks. The Journal of Geology, 10, 555–590.

Dahlgren, R.A., Saigusa, M., and Ugolini, F.C. (2004) The nature, properties and management of soils. Advances in Agronomy, 82, 113–182.

Delvaux, B., Herbillion, A.J., and Vielvoye, L.M. (1989) Characterization of a weathering Sequence of soils derived from volcanic ash in Cameroon—Taxonomic, mineralogical and agronomic implications. Geoderma, 45, 375–388.

Delvaux, B., Herbillion, A.J., Vielvoye, L.M., and Mestdagh, M.M. (1990) Surface properties and clay mineralogy of hydrated halloysitic soil clays. 2. Evidence for the presence of halloysite smectite (H/Sm) mixed-layer clays. Clay Minerals, 25(2), 141–160.

Dessert, C., Dupré, B., François, L.M., Schott, J., Gaillardet, J., Vhakrapani, G.J., and Bajpai, S. (2001) Erosion of Deccan Traps determined by river geochemistry: impact on the global climate and the $^{87}Sr/^{86}Sr$ ratio of seawater. Earth and Planetary Science Letters, 188, 459–474.

Dessert, C., Dupré, B., Gaillardet, J., François, L.M., and Allegre, C.J. (2003) Basalt weathering laws and the impact of basalt weathering on the global carbon cycle. Chemical Geology, 202(3-4), 257–273.

Devereux, S. (2000) Food Insecurity in Ethiopia. A Discussion Paper for DFID. October 2000, http://www.addisvoice.com/wp-content/uploads/2010/03/FoodSecEthiopia4.pdf. Accessed November 4, 2013.

Dudek, T., Cuadros, J., and Fiore, S. (2006) Interstratified kaolinite-smectite: Nature of the layers and mechanism of smectite kaolinization. American Mineralogist, 91, 159–170.

Duzgoren-Aydin, N.S., and Aydin, A. (2003) Chemical heterogeneities of weathered igneous profiles: Implications for chemical indices. Environmental and Engineering Geosciences, 9(4), 363–377.

Duzgoren-Aydin, N.S., Aydin, A., and Malpas, J. (2002) Re-assessment of chemical weathering indices: case study of pyroclastic rocks of Hong Kong. Engineering Geology, 63, 99–119.

Edmond, J.M., Measures, C., McDuff, R.E., Chan, L.H., Collier, R., and Grant, B. (1979) Ridge crest hydrothermal activity and the balances of the major and minor elements in the ocean: The Galapagos data. Earth and Planetary Science Letters, 46, 1–18.

Harnois, L. (1988) The CIW index: A new chemical index of weathering. Sedimentary Geology, 55, 319–322.

Herbillon, A.J., Frankart, R., and Vielvoye, L. (1981) An occurrence of interstratified kaolinite-smectite minerals in a red-black soil toposequence. Clay Minerals, 16, 195–201.

Hijmans, R.J., Cameron, S.E., Parra, J.L., Jones, P.G., and Jarvis, A. (2005) Very high resolution interpolated climate surfaces for global land areas. International Journal of Climatology, 25, 1965–1978.

Hofmann, C., Courtillot, V., Feraud, G., Rochette, P., Yirgu, G., Ketefo, E., and Pik, R. (1997) Timing of the Ethiopian flood basalt event and implications for plume birth and global change. Nature, 389, 838–841.

Holland, H.D. (1984) The Chemical Evolution of the Atmosphere and Oceans. Princeton University Press, New Jersey.

Iriarte, I., Petit, S., Huertas, J., Fiore, S., Grauby, O., Decarreau, A., and Linares, J. (2005) Synthesis of kaolinite with a high level of Fe^{3+} for Al substitution. Clay and Clay Minerals, 53, 1–10.

Jenny, H. (1941) Factors of Soil Formation. McGraw-Hill, New York.

Johannsen, A. (1931) A descriptive petrography of the igneous rocks, vol. 1, 267 pp. Chicago University Press, Illinois.

Kelsey, C.H. (1965) Calculations of the CIPW norm. Mineralogical Magazine, 34, 276–282.

Kieffer, B., Arndt, N., Lapierre, H., Bastien, F., Bosch, D., Pecher, A., Yirgu, G., Ayalew, D., Weis, D., Jerram, D.A., Keller, F., and Meugniot, C. (2004) Flood and shield basalts from Ethiopia: Magmas from the African Superswell. Journal of Petrology, 45(4), 793–834.

Kirkup, L. (2012) Data analysis for physical scientists: Featuring Excel®, Second ed. Cambridge University Press, U.K.

Le Blond, J.S., Williamson, B.J., Horwell, C.J., Monro, A.K., Kirk, C.A., and Oppenheimer, C. (2008) Production of potentially hazardous respirable silica airborne particulate from the burning of sugarcane. Atmospheric Environment, 42, 5558–5568.

Ma, J.L., Wei, G.J., Xu, Y.G., Long, W.G., and Sun, W.D. (2007) Mobilization and re-distribution of major and trace elements during extreme weathering of basalt in Hainan Island, South China. Geochimica et Cosmochimica Acta, 71, 3223–3237.

Malden, P.J., and Meads, R.E. (1967) Substitution by iron in kaolinite. Nature, 215, 844–846.

McLennan, S.M. (1993) Weathering and global denudation. Journal of Geology, 101, 295–303.

Meunier, A. (2005) Clays, 472 pp. Springer, Berlin.

Mohr, P. (1983) Ethiopian flood basalt province. Nature, 303, 577–584.

Mohr, P., and Zanettin, B. (1988) The Ethiopian flood basalt province. In J.D. Macdougall, Ed., Continental Flood Basalts, pp. 63–110. Kluwer Academic, Dordrecht.

Nesbitt, H.W., and Young, G.M. (1982) Proterozoic climates and plate motions inferred from major chemistry of lutites. Nature, 299, 715–717.
Ohta, T., and Arai, H. (2007) Statistical empirical index of weathering in igneous rocks: A new tool for evaluating the degree of weathering. Chemical Geology, 240, 280–297.
O'Neil, J., Francis, D., and Carlson, R.W. (2011) Implications of the Nuvvuagittuq Greenstone Belt for the formation of the early earth. Journal of Petrology, 52, 985–1009.
Óskarsson, B., Riishuus, M.S., and Arnalds, Ó. (2012) Climate-dependent chemical weathering of volcanic soils in Iceland. Geoderma, 189-190, 635–651.
Plançon, A. (2002) New modelling of X-ray diffraction by disordered lamellar structures, such as phyllosilicates. American Mineralogist, 87, 1672–1677.
Price, J.R., and Velbel, M.A. (2003) Chemical weathering indices applied to weathering profiles developed on heterogeneous felsic metamorphic parent rocks. Chemical Geology, 202, 397–416.
Rasmussen, C., Dahlgren, R.A., and Southard, R.J. (2010) Basalt weathering and pedogenesis across an environmental gradient in the southern Cascade Range, California, USA. Geoderma, 154, 473–485.
Retallack, G.J. (2001) Soils of the Past: An Introduction to Paleopedology. Blackwell, Malden, Massachusetts.
Righi, D., Terribile, F., and Petit, S. (1999) Pedogenic formation of kaolinite-smectite mixed layers in a soil toposequence developed from basaltic parent material in Sardinia (Italy). Clays and Clay Minerals, 47, 505–514.
Ryan, P.C., and Huertas, F.J. (2009) The temporal evolution of pedogenic Fe-smectite to Fe-kaolin via interstratified kaolin-smectite in a moist tropical soil chronosequence. Geoderma, 151, 1–15.
Sigfusson, B., Gislason, S.R., and Paton, G.I. (2008) Pedogenesis and weathering rates of a histic andosol in Iceland: Field and experimental soil solution study. Geoderma, 144, 572–592.
Singh, B., and Gilkes, R.J. (1993) The recognition of amorphous silica in indurated soil profiles. Clay Minerals, 28, 461–474.
Szilas, K., and Garde, A.A. (2013) Mesoarchaean aluminous rocks at Storø, southern West Greenland: New age data and evidence of premetamorphic seafloor weathering of basalts. Chemical Geology, 354, 124–138.
Taylor, S.R., and McLennan, S.H. (1985) The Continental Crust: Its composition and evolution, 312pp. Blackwell, Oxford.
Taylor, S.R., McLennan, S.M., and McCulloch, M.T. (1983) Geochemistry of loess, continental crust composition and crustal composition and crustal model ages. Geochimica et Cosmochimica Acta, 47, 1897–1905.
Teferi, E., Uhlenbrook, S., Bewket, W., Wenninger, J., and Simane, B. (2010) The use of remote sensing to quantify wetland loss in the Choke Mountain range, Upper Blue Nile basin, Ethiopia. Hydrology and Earth System Sciences, 14, 2415–2428, http://dx.doi.org/10.5194/hess-14-2415-2010.
Tolosana-Delgado, R., Otero, N., Pawlowsky-Glahn, V., and Soler, A. (2005) Latent compositional factors in the Llobregat River Basin (Spain) hydrogeochemistry. Mathematical Geology, 37, 681–702.
Truckenbrodt, W., Kotschoubey, B., and Schellmann, W. (1991) Composition and origin of the clay cover on Northern Brazilian laterites. Geologische Rundschau, 80, 591–610.
Van de Wauw, J., Baert, G., Moeyersons, J., Nyssen, J., De Geyndt, K., Taha, N., Zenebe, A., Poesen, J., and Deckers, J. (2008) Soil-landscape relationships in the basalt-dominated highlands of Tigray, Ethiopia. Cantena, 75, 117–127.
Vingiani, S., Righi, D., Petit, S., and Terribile, F. (2004) Mixed-layer kaolinite-smectite minerals in a red-black soil sequence from basalt in Sardinia (Italy). Clays and Clay Minerals, 52, 473–483.
Viti, C., Luperi, M., and Reginelli, M. (2007) Weathering sequence of rhyolitic minerals: the kaolin deposit of Torniella (Italy). Nbeues Jahrbuch für Mineralogie Abhandlugen, 182/3, 203–213.
Weaver, C.E., Wampler, J.M., and Pecuil, T.E. (1967) Mössbauer analysis of iron in clay minerals. Science, 156, 504–510.
Zhang, Y., Pe-Piper, G., and Piper, D.J.W. (2014) Sediment geochemistry as a provenance indicator: Unravellling the cryptic signatures of polycyclic sources, climate change, tectonism and volcanism. Sedimentology, 61, 383–410.

Manuscript received August 19, 2014
Manuscript accepted December 30, 2014
Manuscript handled by Lynda Williams